Forest Ecology and Management 499 (2021) 119638

Contents lists available at ScienceDirect

Forest Ecology and Management

journal homepage: www.elsevier.com/locate/foreco

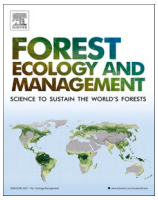

Important meteorological predictors for long-range wildfires in China

Fengjun Zhao [a,b], Yongqiang Liu [a,*]

[a] Center for Forest Disturbance Science, USDA Forest Service, Athens, GA, USA
[b] Research Institute of Forest Ecology, Environment and Protection, Chinese Academy of Forestry and Key Laboratory of Forest Protection of National Forestry and Grassland Administration, Beijing, China

ARTICLE INFO

Keywords:
Fire-meteorological relationship
Correlation
Regression model
Fire prediction skill
Drought index

ABSTRACT

Wildfire predictions provide useful information for fire management planning and implementation. Temperature and precipitation have been used as the primary meteorological predictors for wildfires in China. This study is to improve the prediction skills of long-range (monthly, seasonal, and annual) wildfires in China by identifying other important meteorological predictors. Provincial data during 1999–2020 were used to calculate the correlations between fire properties (fire count and burned area) and meteorological variables of maximum temperature, precipitation, relative humidity, wind speed, and vapor pressure deficit (VPD) and drought indices of Keetch-Bryam Drought Index (KBDI), Palmer Drought Severity Index (PDSI), and Standardized Precipitation Index (SPI). The fitting rates of the linear regression fire prediction models were compared among these meteorological variables and drought indices. The results indicate that the number of provinces with significant correlations and / or high fitting rates is the largest with VPD for monthly fires, KBDI for seasonal fires, and KBDI, PDSI, and SPI for annual fires. The number is larger in Northeast, Central, and South China than in other China regions. The number is comparable between spring and other seasons for KBDI but often smaller in spring for meteorological variables. The number is generally smaller for burned areas than fire count. It is concluded that the skills of long-range fire predictions are expected to be improved in many provinces of China by using VPD and KBDI as well as some other drought indices.

1. Introduction

Wildfires are caused by both natural and human factors with severe ecological, environmental, social, and economic consequences (Moritz et al., 2014; Liu et al., 2014; Doerr and Santín, 2016; Steelman, 2016; Reddington et al., 2019). With the rapid increase in population and urbanization, wildfires are gradually getting closer to the wildland–urban interface, increasing tragic loss of human lives and properties (Gill and Stephens, 2009; Nagy et al., 2018; Molina-Terrén et al., 2019; Bo et al., 2020; Brown et al., 2020). Wildfires have increased in many regions of the world in recent decades (Westerling et al., 2006; Flannigan et al., 2009; Holdena et al., 2018; Zhao et al., 2020), and will likely become more frequent and intense in the future as a consequence of the projected climate change (Flannigan et al., 2009; Liu et al., 2010; Abatzoglou and Williams, 2016; Schoennagel et al., 2017).

Wildfire danger prediction is needed for fire and land management to plan and implement fire prevention, suppression, and impact mitigation. Meteorological conditions are often used as predictors for wildfires (Westerling et al., 2003; Goodrick et al., 2017; Turco et al., 2018; Bedia et al., 2018). The World Meteorological Organization defines meteorological forecast at various ranges, including short range (daily and weekly) and long range (monthly, seasonal, and annual) (http://www.wmo.int/pages/prog/www/DPS/GDPS-Supplement5-AppI-4.html). Fire predictions are provided at different ranges accordingly. For example, the United States National Interagency Coordination Center (NICC) (https://www.predictiveservices.nifc.gov), Canada Natural Resources (https://cwfis.cfs.nrcan.gc.ca/maps/forecasts), and Australia's Bushfire and Natural Hazard Cooperative Research Centre (https://www.bnhcrc.com.au/hazardnotes/85) provide daily, weekly, bi-weekly, monthly, and seasonal fire potential prediction and outlook products.

Predictions of short-range fires are based on fire-meteorological relationships mainly reflecting the dynamical controls of weather on fire ignition and spread probability (Potter, 2012). The weather conditions for fire danger are described essentially by meteorological variables (also called meteorological elements) such as temperature, precipitation, humidity, and wind (Koutsias et al., 2013). Meteorological variables are used either directly as predictors in fire prediction models or as

* Corresponding author.
E-mail address: yongqiang.liu@usda.giv (Y. Liu).

https://doi.org/10.1016/j.foreco.2021.119638
Received 6 May 2021; Received in revised form 13 August 2021; Accepted 15 August 2021
0378-1127/Published by Elsevier B.V.

Table 1
Regions and provinces in China for wildfire analysis, together with regional temperature (T) and precipitation (R).

Region	Abbre.	Province	Abbre.	T (°C)	R (mm)
Northeast	NE	Daxing'anling	DA	<6	500–600
		Heilongjiang	HL		
		Jilin	JL		
		Liaoning	LN		
North	NC	Inner Mongolia	IM	8–10	400–500
		Hebei	HB		
		Shanxi	SX		
		Shangdong	SD		
Central	CC	Henan	HA	16–20	1000–1200
		Anhui	AH		
		Hubei	HU		
		Jiangsu	JS		
		Zhejiang	ZJ		
South	SC	Hunan	HN	>20	>1600
		Jiangxi	JX		
		Fujian	FJ		
		Guangdong	GD		
		Guangxi	GX		
		Hainan	HI		
Southwest	SW	Sichuan	SC	14–16	1000–1200
		Guizhou	GZ		
		Yunnan	YN		
Tibet	TI	Tibet	TI	10–12	700–800
Northwest	NW	Shannxi	SH	8–10	<400
		Gansu	GS		
		Qinghai	QH		
		Ningxia	NX		
		Xinjiang	XJ		

essential information for calculating fire indices in operational fire risk assessment systems such as the U.S. Fire Danger Rating System (NFDRS) (Deeming et al., 1977), the Canadian Forest Fire Weather Index (FWI) System (Van Wagner, 1987), and the Australian McArthur Forest Fire Danger Index (FFDI) (McArthur 1967).

Predictions of long-range fires, on the other hand, are based on the fire-meteorological relationships reflecting the impacts of abnormal weather conditions (Goodrick and Hanley, 2009; Abatzoglou and Kolden, 2013; Gudmundsson, et al., 2014), atmospheric circulation anomalies (Zhao and Liu 2019), and oceanic events such as El Nino / La Nina (Chen et al., 2011; Liu 2006; Chen et al., 2017; Harris et al., 2014; Yao et al., 2017; Fang et al., 2021) on fire statistics during one or more fire seasons. Droughts are the most typical abnormal weather conditions for wildfires. Drought indices have been widely used to predict long-range wildfires (Gudmundsson et al., 2014; Marcos et al., 2015; Littell et al., 2016; Shawki et al., 2017). Drought indices are constructed by more than one meteorological variable [e.g., the Palmer Drought Severity Index (PDSI) (Palmer, 1965; Dai, 2011) and Keetch-Byram Drought Index (KBDI) (Keetch and Byram, 1968)] or converted from a single meteorological variable [e.g., the Standardized Precipitation Index (SPI) (McKee et al., 1993)]. Drought indices are often an integrated part of a fire risk assessment system. For example, the US NFDRS, the Canadian FWI, and the Australian FFDI use KBDI or a specific drought code drought factor to assess monthly and seasonal fire danger. The long-range fire predictions provided by NICC use temperature and precipitation anomalies, drought conditions, and El Nino / La Nina events as major factors (https://www.predictiveservices.nifc.gov/NMAC%20Weather%20Outlook.mp4).

China is one of the regions in the world with large wildfire activity, where operational long-range regional fire predictions are provided by China's National Climate Center (http://cmdp.ncc-cma.net/drought/fm/) and other institutions at national and regional levels and by local meteorological services and other agencies at the provincial level. Similar to many other regions of the world (Spessa et al., 2015; Lima et al., 2018), the long-range fire predictions in China are made based mainly on abnormal temperature and precipitation, together with atmospheric circulation and sea surface temperature anomalies. However, other meteorological variables and many drought indices have been found to be closely related to wildfires in different regions of the world, including China (Tian et al., 2003; Jia et al., 2011). For example, vapor pressure deficit (VPD) was found recently to be a very useful element for fire prediction (Sedano and Randerson, 2014; Seager et al., 2015). It is valuable for potentially improving the skills of the long-range fire predictions in China by comparing these meteorological variables and drought indices with traditionally used predictors of temperature and precipitation and understanding their relative importance for predicting wildfires at different time scales (monthly, seasonal, etc.).

Both fires and meteorological conditions change in space and time (Drobyshev et al., 2012; Li et al., 2013; Assal et al., 2016; Zhou et al., 2017). Most fires occur in eastern China, where climate is controlled by

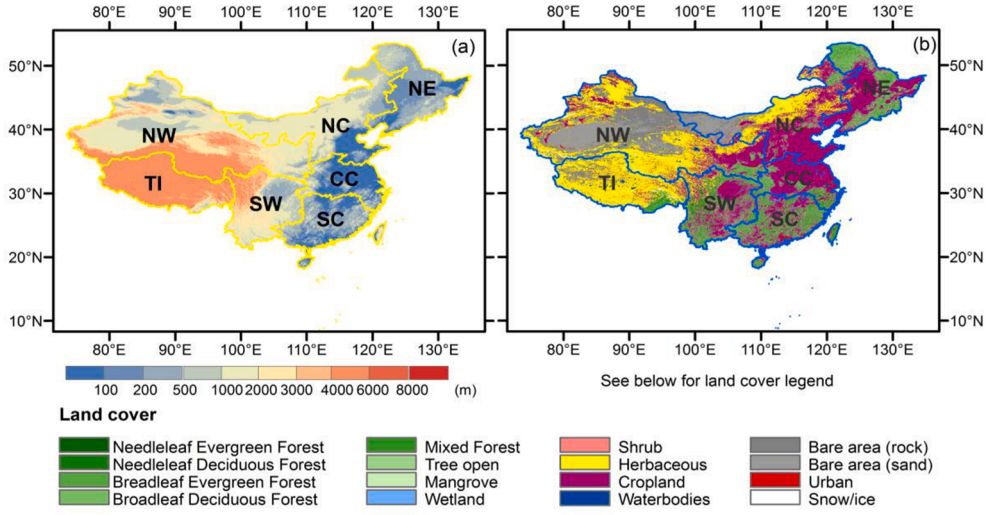

Fig. 1. Study area. (a) Elevation. (b) Land cover. The regions are Northeast (NE), North (NC), Central (CC), South (SC), Southwest (SW), Tibet (TI), and Northwest (NW) China. (The data used to produce this figure were obtained from https://globalmaps.github.io/).

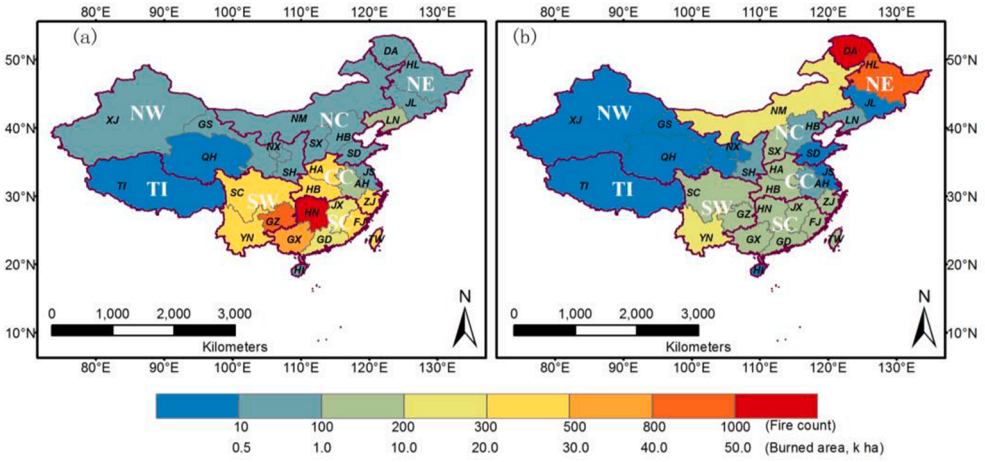

Fig. 2. Spatial distributions of annual forest fires in China. (a) Fire count. (b) Burned area. The letters in yellow and black are regions and provinces, respectively (see Table 1 for their full names). (For interpretation of the references to colour in this figure legend, the reader is referred to the web version of this article.)

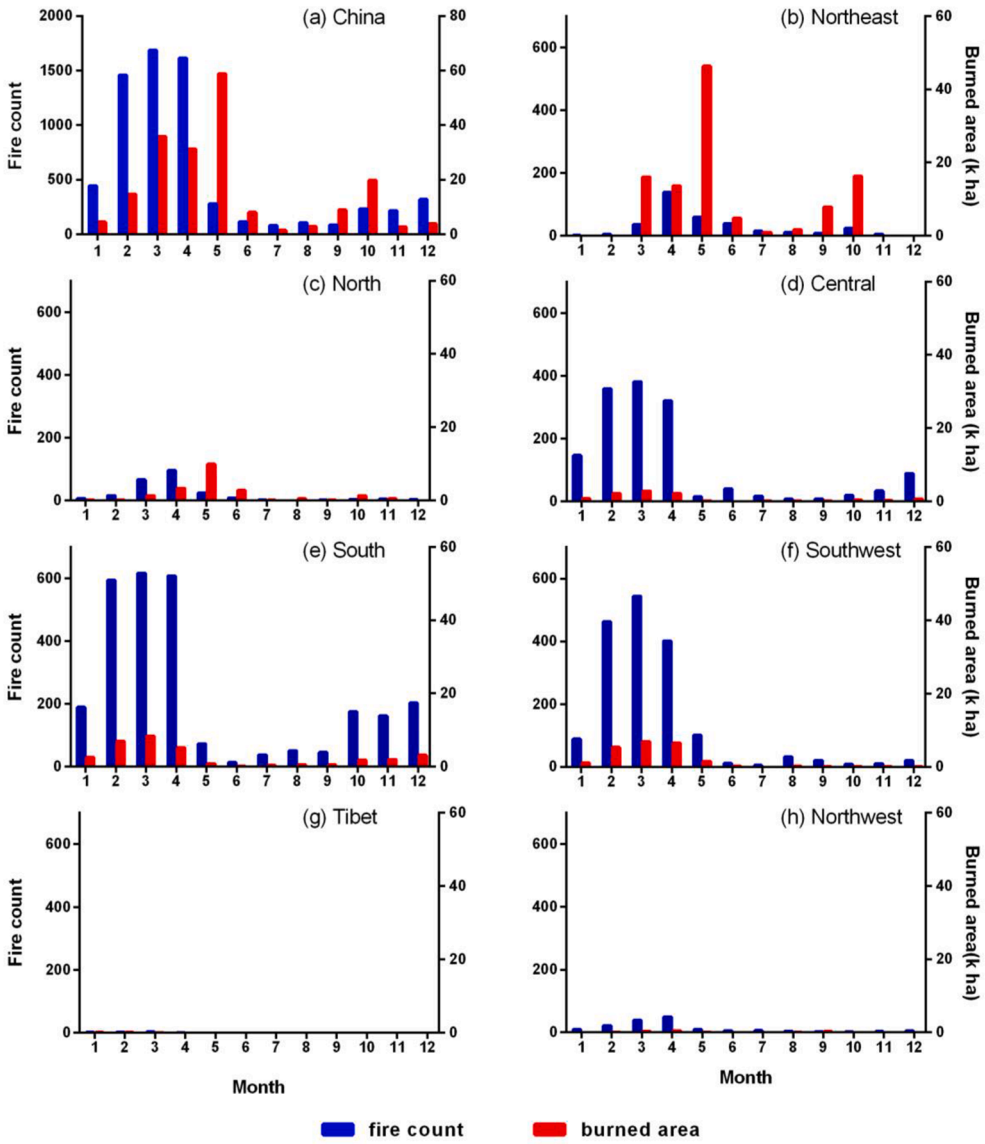

Fig. 3. Monthly fire count and burned area in China (a), Northeast (b), North (c), Central (d), South (e), Southwest (f), Tibet (g), and Northwest (h). (see Table 1 and Fig. 2 for full names and locations of these regions.)

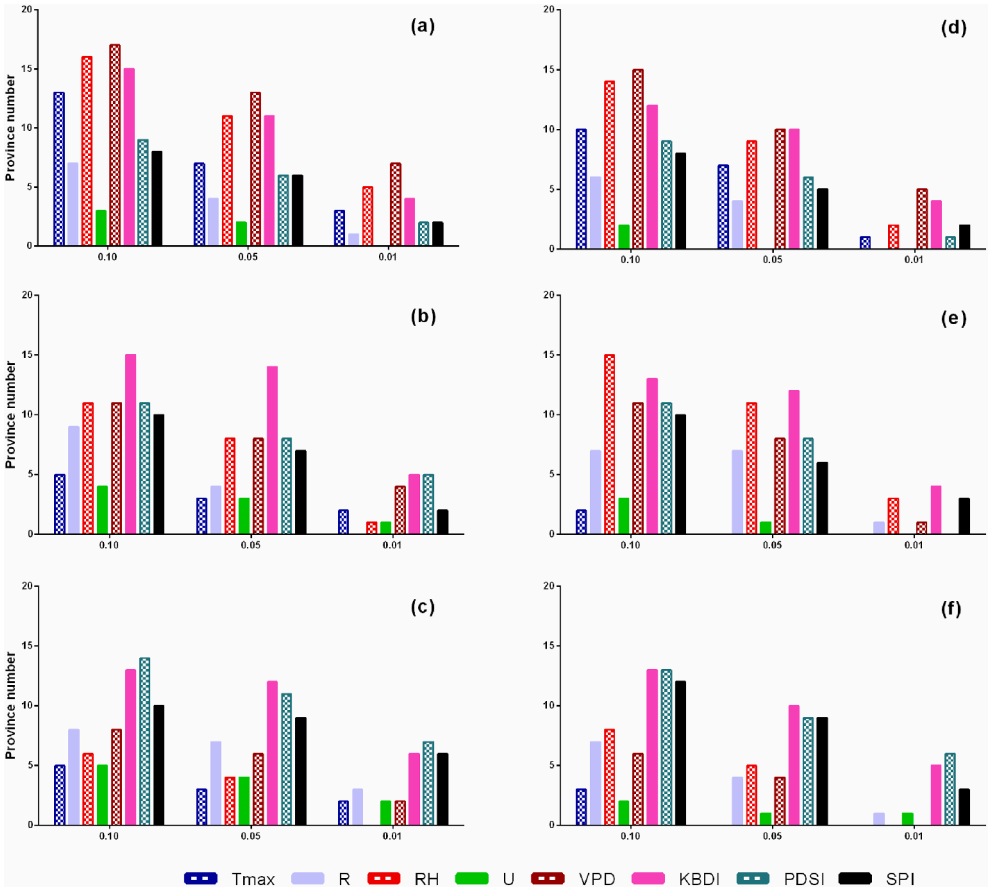

Fig. 4. Number of provinces with significant fire-meteorological correlations. (a-c) Monthly, seasonal, and annual fire count. (d-f) The corresponding burned area. T_{max}, *R*, *RH*, *U*, *VPD*, *KBDI*, *PDSI*, and *SPI* are maximum temperature, precipitation, relative humidity, vapor pressure deficit, Keetch-Byram Drought Index, Palmer Drought Severity Index, and Standardized Precipitation Index.

dynamical and variable monsoons. Wildfires are much more frequent in southern than northern portions of eastern China, while burned area has an opposite pattern (Lv et al., 2006; Tian et al., 2013; Li et al., 2015; Chen et al., 2017). Major fires in many China regions occur in more than one season (Tian et al., 2013, 2015; Chen et al., 2017). For example, northeastern China has large fires in both spring and fall. Wildfires in China vary remarkably from one year to another (Yi et al., 2017). The spatial and temporary variations in both wildfire and climate lead to complex fire-meteorological relationships in China (Guo et al., 2016; Ye et al., 2017; Yao et al., 2017; Du et al., 2021). It is not clear how the variations affect the important meteorological predictors for long-range fires in China at different time scales.

In addition to weather and climate conditions, fires are also impacted by non-natural factors such as human activity and fire management policy. Human related incidents are one of the causes for fire ignition and fire occurrence (i.e., fire number), while burned area is partially determined by fire suppression. Since the 1987 Black Dragon Fire in Daxing'anling (Cahoon et al., 1994), China has implemented a strict forest fire suppression policy (Zhao et al., 2009). This may undermine the fire-meteorological relationships. It is valuable to evaluate this impact by comparing fire-meteorological relationships between different fire properties.

The purpose of this study is to understand the relative importance of various meteorological variables and drought indices as predictors for long-range wildfires in China and the dependence on geographic region, fire season, and fire property. The measured and derived meteorological conditions, including meteorological variables of maximum temperature, precipitation, relative humidity, wind speed, and vapor pressure deficit and drought indices including KBDI, PDSI, and SPI were used to analyze correlations with fire number and burned area from each province of China. Regression models were formed based on the correlations to predict long-range fires. The important predictors were identified through comparing the correlations and prediction fitting rates among all meteorological variables and drought indices. Considering that operational fire predictions at annual scale are not currently provided in China but may become possible in the foreseeable future with the improving climate prediction skills, the long-range predictions of annual fires were also analyzed in addition to monthly and seasonal fire predictions. The results from this study are expected to provide useful information for improving the skills of long-range fire predictions not only in China but also in other regions of the world.

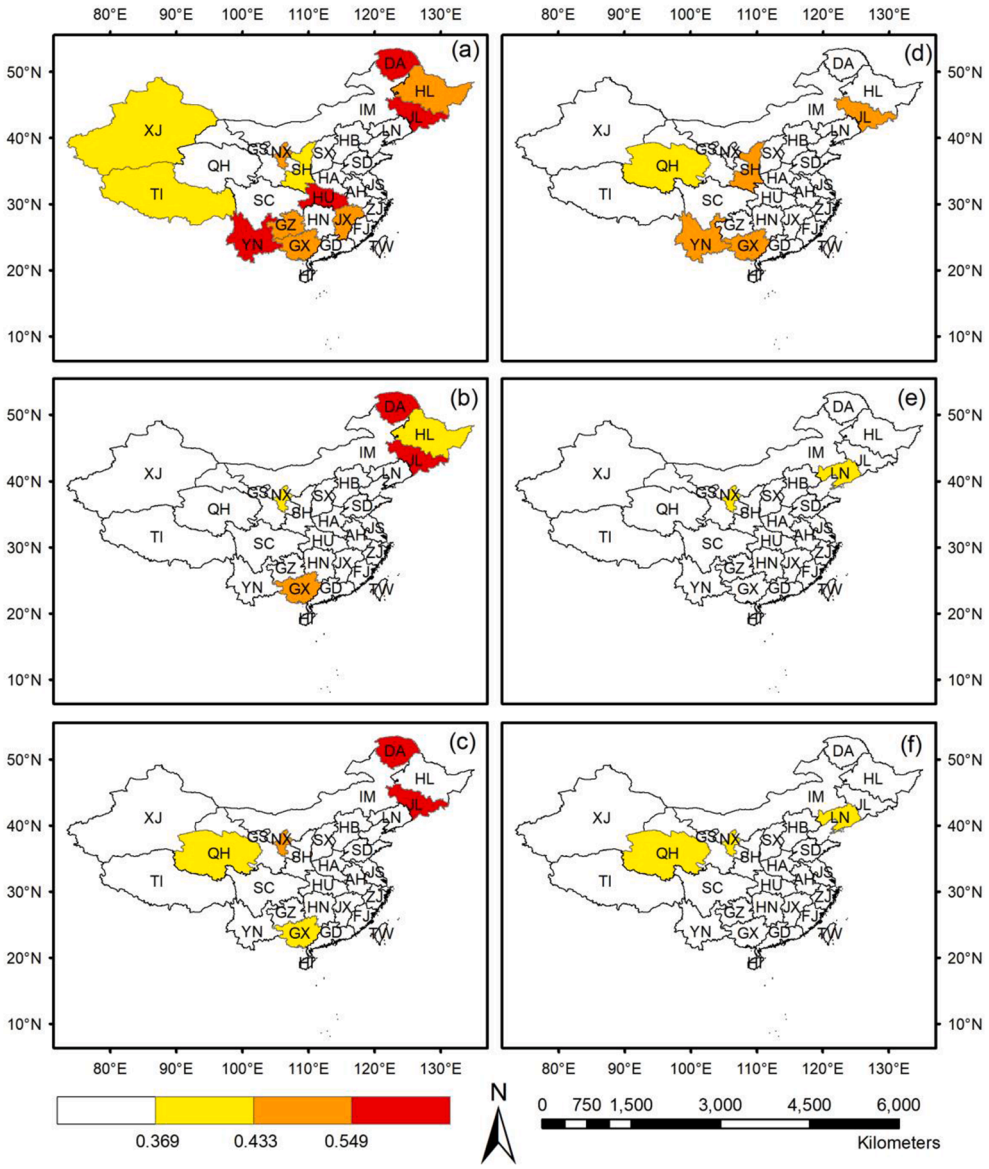

Fig. 5. Provinces with significant fire-maximum temperature correlations. (a-c) monthly, seasonal, and annual fire count. (d-f) The corresponding burned area. The critical values are 0.369 ($p < 0.1$), 0.433 ($p < 0.05$), and 0.549 ($p < 0.01$).

2. Methods

2.1. Study area

The study area was mainland China with an area of 9.6 million km^2. It consists of 27 provinces (Table 1). The four municipalities of Beijing, Tianjin, Shanghai, and Chongqing and the two special administrative regions of Hong Kong and Macao were included in the corresponding surrounding or nearby provinces. A major boreal forest of 77 thousand km^2 on the Heilongjiang and Inner Mongolia border called Daxing'anling has large and intense fires, and fire prevention in this area is critical for fire management in China (Tian et al., 2013). Thus, this area was analyzed separately and regarded as a "province" in this study, leading to a total number of provinces at 28. According to the spatial patterns of topography, vegetation, and climate to be described below, China was divided into seven regions (Fig. 1 and Table 1): Northeast (NE), North (NC), Central (CC), South (SC), Southwest (SW), Tibet (TI), and Northwest (NW). The following terms are used for convenience of description: "eastern China" (including NE, NC, CC, SC, and SW), "western China" (TI and NW), "northern China" (NE and NC), and "southern China" (CC, SC, and SW).

China has a three-step topography with increasing elevations from east to west (Fig. 1a): Step 1 - the coastal areas including NE, CC, SC, and eastern NC mostly below 200 m; Step 2 - SW and western NC with elevations up to 3000 m; and Step 3 - western China with varied elevations of 3000–6000 m in TI and 1000–3000 m in NW.

Forests (Fig. 1b) cover about 23% of lands in China, with needle and broadleaf trees distributed mainly in SC, SW, northern and eastern NE, southern CC, and elevated mountains in TI and NW (FRC, 2014). Grasslands are distributed mainly in northern NC, northern TI, and some sparse NW areas. Croplands are mainly in CC, southern NC, southern NE, and northern SW. Deserts and dry lands are mainly in southern and eastern NW.

Eastern China is under control of the East Asian monsoon climate, which is extremely wet and warm during summers and dry and cold during winters. Western China mainly has a continental climate, which is dry with cold winters and warm summers. Annual temperature (Table 1) decreases from over 20 °C in SC to 8–10 °C in NW and below 6 °C in NE. Annual precipitation gradually decreases from south to north, with more than 1600 mm in SC and less than 400 mm in NW. The

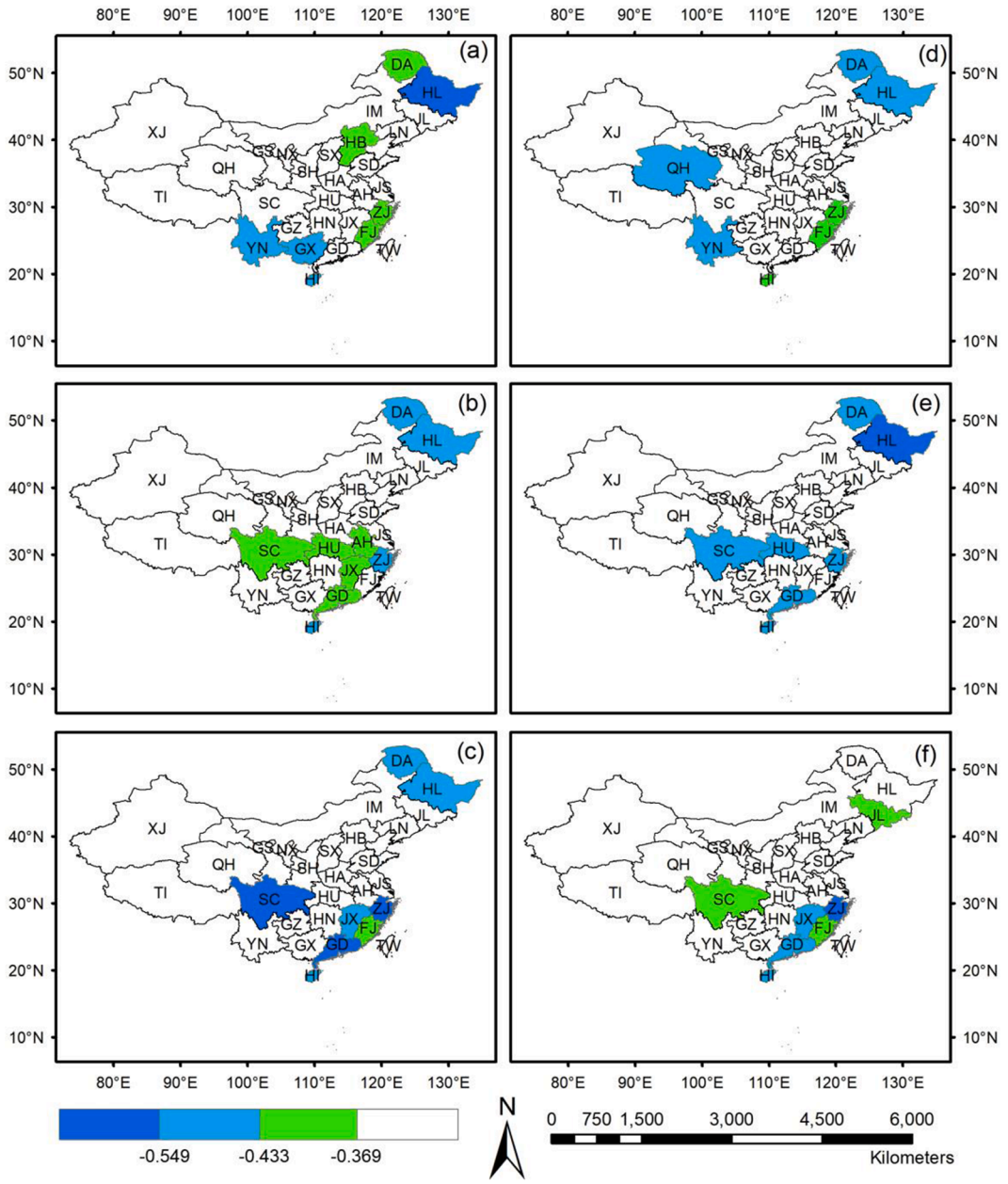

Fig. 6. Provinces with significant fire-precipitation correlations. (a-c) monthly, seasonal, and annual fire count. (d-f) The corresponding burned area. The critical values are 0.369 ($p < 0.1$), 0.433 ($p < 0.05$), and 0.549 ($p < 0.01$).

annual temperature and precipitation were calculated based on the data described below.

2.2. Data

2.2.1. Fires

Unlike many other countries such as the United States, historical fire data reported from fire management is very limited in China (Lv et al., 2006; Zhang et al., 2016). Most data analyses were conducted at the national or regional level for annual fires. Remote sensing has been a very useful tool to obtain high-resolution spatial distributions and frequent temporal variability of fires in China (Li et al., 2013; Tian et al., 2013; Chen et al., 2017). However, the provincial and regional burned areas obtained using this technique were found to be significantly different from those from historical data with large regional inconsistencies (Li et al., 2015; Yi et al., 2017), partially because of a large number of small fires in China that were difficult to detect due to timing of satellite overpass. The lack of historical fire data has been one of the major limitations for understanding the spatial (e.g., provinces across China) and temporal (e.g., monthly variability) features of fire-meteorological relationships in China.

The fire dataset used in this study was developed recently by the China National Forestry and Grassland Administration and obtained from the China National Forest Fire Statistical System (accessible after registering at http://60.205.191.66/FireReport/Account/LogOn?returnUrl=%2FFireReport%2F). The fire data (*F*) included monthly fire count (*FC*) and burned area (*FA*) for each province, together with information on casualties, economic loss, and suppression personnel during 1999–2019. Seasonal and annual *F* values were obtained by adding the monthly values. An early version of the dataset for the period of 1999–2017 was used by us to analyze the atmospheric circulation patterns for regional fires in eastern China (Zhao and Liu 2019).

Fires are ignited by either lightning or human causes, and meteorological conditions play important roles in fire ignition mainly by

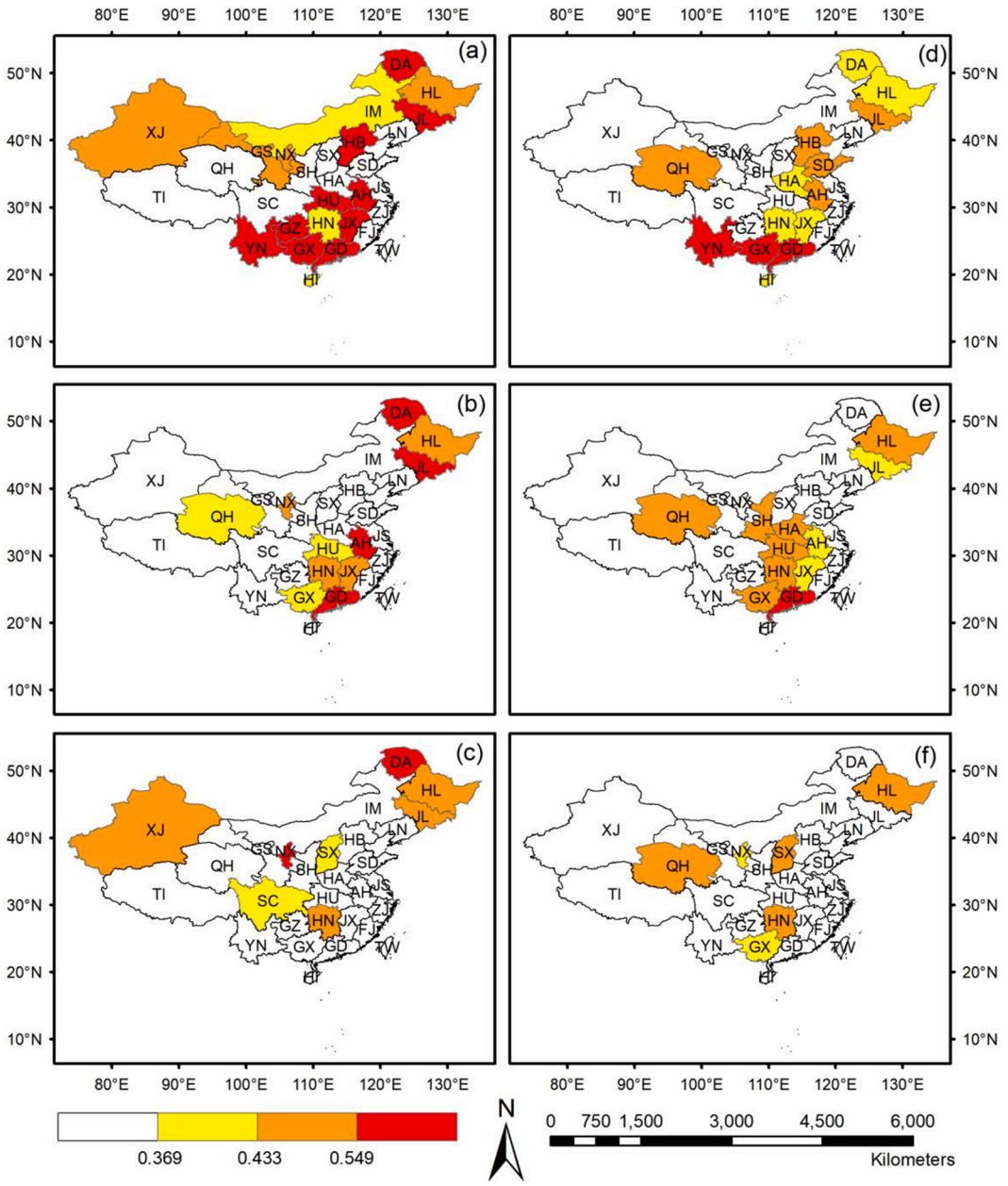

Fig. 7. Provinces with significant fire-vapor pressure deficit correlations. (a-c) monthly, seasonal, and annual fire count. (d-f) The corresponding burned area. The critical values are 0.369 ($p < 0.1$), 0.433 ($p < 0.05$), and 0.549 ($p < 0.01$).

lightning (Dowdy and Mills, 2012). However, the fire data did not include information on fire causes. Thus, all fire data were used. In addition, the fire data series were only 21 years long. Some other fire datasets in China (Lv et al., 2006; Yi et al., 2017; Yao et al., 2017) are longer but without monthly and / or provincial resolution.

2.2.2. *Meteorological variables*

Daily observed meteorological data during 1999–2019 were obtained from the China Meteorological Science Data Sharing Service Network (http://cdc.nmic.cn). The original dataset included values from more than 800 weather stations across China. It would be ideal to use fire and meteorological data from the same or close locations. However, the fire data were accumulated for each province without location information on individual fires. Thus, we had to average data from weather stations within a province. Considering that wildfires occurred on vegetated lands, only about 600 weather stations located in the areas covered by forest, grass, and shrub were used based on the global vegetation coverage obtained from the International Geosphere-Biosphere Program (IGBP) (https://globalmaps.github.io/).

Five meteorological variables were analyzed, including measured maximum air temperature (T_{max}) at 2 m above ground, precipitation (R), and wind speed (U) at 10 m above ground, and derived relative humidity (RH) from the measured specific humidity and temperature, and VPD from temperature and RH (Seager et al., 2015). The monthly, seasonal, and annual values of the variables, together with $KBDI$ to be described below, were obtained by averaging the daily values over the

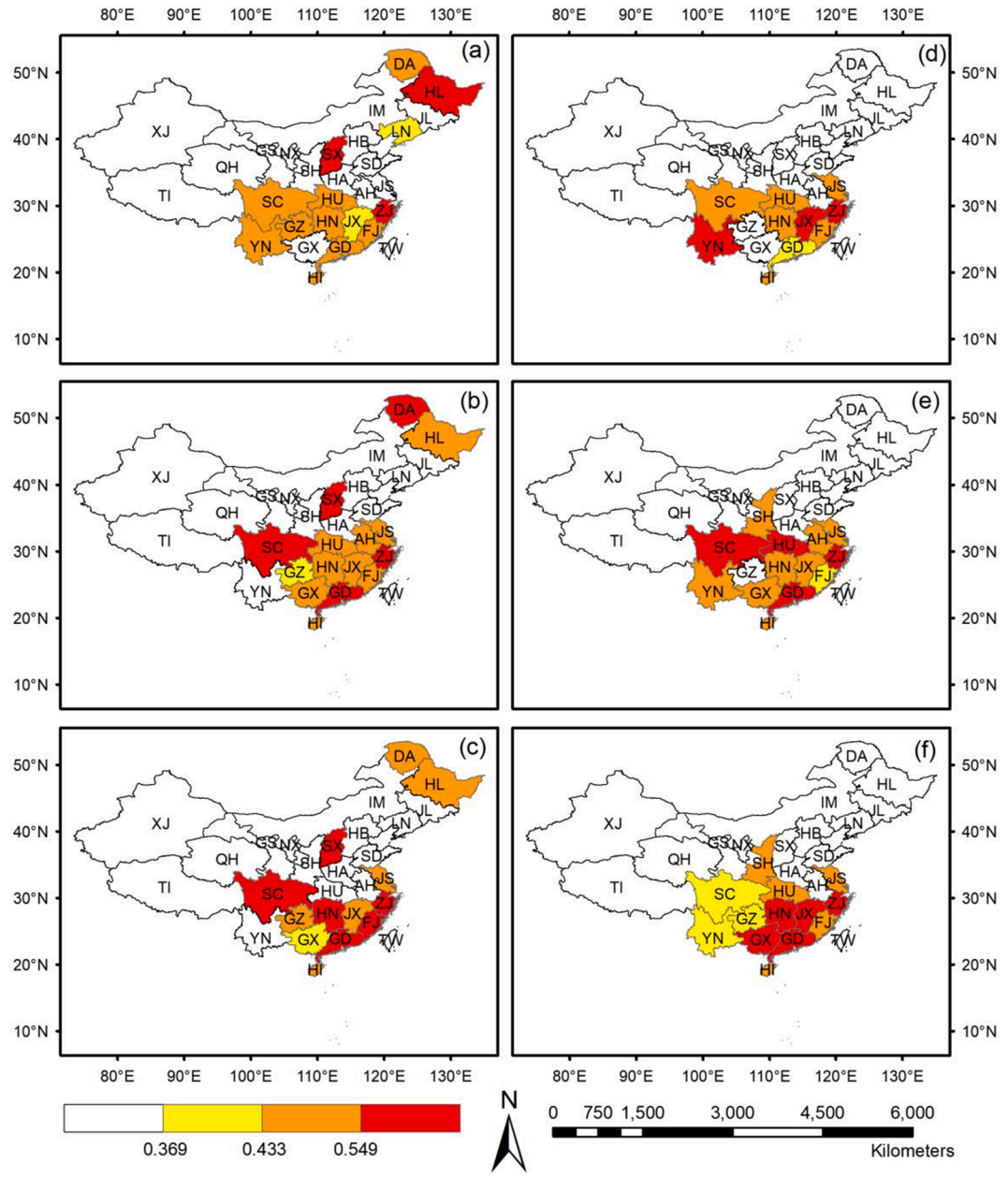

Fig. 8. Provinces with significant fire-KBDI correlations. (a-c) monthly, seasonal, and annual fire count. (d-f) The corresponding burned area. The critical values are 0.369 ($p < 0.1$), 0.433 ($p < 0.05$), and 0.549 ($p < 0.01$).

corresponding time periods.

2.2.3. Drought indices

Three drought indices were analyzed. *KBDI*, a drought index developed specifically to measure fire potential, was calculated daily using:

$$dQ = \frac{10^{-3}(800 - Q_0)[0.968e^{0.0486T_{max}} - 8.3]d\tau}{1 + 10.88e^{-0.0441R_a}} \quad (1)$$

$$Q = Q_0 + dQ - dR \quad (2)$$

where Q and Q_0 are KBDI of the current and previous day, respectively; dQ is KBDI incremental rate; dR daily precipitation; R_a the mean annual precipitation; and $d\tau$ a time increment set equal to one day. An adjustment was made so that $dQ = 0$ when $T \leq 50^\circ F$ ($10\,^\circ C$). In addition, only the portion of daily precipitation above the net accumulated precipitation of 0.5 cm (0.20 in.) was used (only applied to the first day for a rain event of multiple days).

PDSI, a popularly used drought index, was obtained from a global gridded monthly dataset with 0.5° resolution (van der Schrier et al., 2013; Osborn et al., 2017). The value of each province was obtained by averaging the values at nearby grid points with a weight factor inversely proportional to the distance. *SPI*, a popular precipitation deficit measure, was calculated at 1, 3, and 12 month scales using a function available in the NCAR Command Language (NCL) (https://www.ncl.ucar.edu).

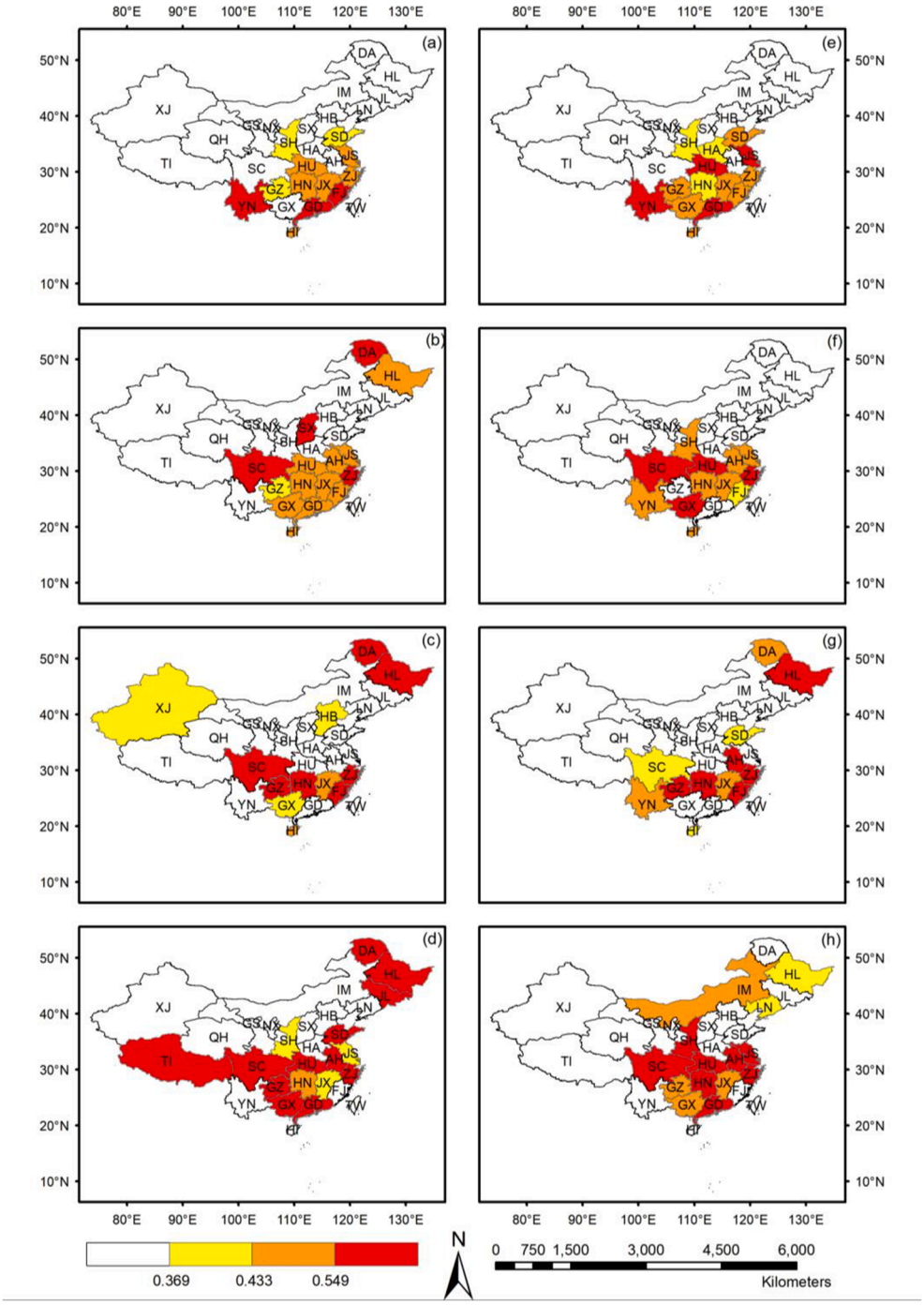

Fig. 9. Provinces with significant seasonal fire-KBDI correlations. (a-d) are for winter, spring, summer, and fall of fire count. (e-h) are the corresponding burned area. The critical values are 0.369 ($p < 0.1$), 0.433 ($p < 0.05$), and 0.549 ($p < 0.01$).

Table 2
Distributions of the number of provinces and percent with a prediction fitting rate greater than the random rate of 33% with regions. The number in parentheses is for a fitting rate greater than 71%.

Region	Province number	Fire count						Burned area					
		Monthly		Seasonal		Annual		Monthly		Seasonal		Annual	
		Num	Percent	Num	Percent	Num	Percent	Num	Percent	Num	Percent	Num	Percent
NE	4	4 (2)	100 (50)	4 (3)	100 (75)	3 (2)	75 (50)	3 (0)	75 (0)	4 (3)	100 (75)	3 (1)	75 (25)
NC	4	4 (3)	100 (75)	3 (1)	75 (25)	2 (1)	50 (25)	2 (1)	50 (25)	3 (0)	75 (0)	2 (0)	50 (0)
CC	5	4 (3)	80 (60)	5 (3)	100 (60)	5 (4)	100 (80)	4 (4)	80 (80)	5 (2)	100 (40)	5 (3)	100 (60)
SC	6	6 (5)	100 (83)	6 (3)	100 (50)	6 (2)	100 (33)	5 (5)	83 (83)	6 (5)	100 (83)	6 (4)	100 (67)
SW	3	3 (3)	100 (100)	2 (1)	66 (33)	2 (1)	66 (33)	3 (1)	100 (33)	2 (0)	67 (0)	3 (1)	100 (33)
TI	1	0 (0)	0 (0)	0 (0)	0 (0)	0 (0)	0 (0)	0 (0)	0 (0)	0 (0)	0 (0)	0 (0)	0 (0)
NW	5	4 (2)	80 (40)	3 (1)	60 (20)	3 (0)	60 (0)	3 (2)	60 (40)	3 (1)	60 (20)	3 (2)	60 (40)
China	28	25 (18)	89 (64)	23 (12)	82 (43)	21 (10)	75 (36)	20 (13)	71 (46)	23 (11)	82 (39)	22 (11)	79 (39)

Table 3
Distribution of the number of provinces and percent with a prediction fitting rate greater than the random rate of 33% with meteorological variables and drought indices. The number in parentheses is for a fitting rate greater than 71%.

Variable	Fire count			Burned area		
	Monthly	Seasonal	Annual	Monthly	Seasonal	Annual
Tmax	7 (5)	1 (0)	2 (1)	7 (4)	2 (1)	1 (0)
R	3 (3)	3 (1)	4 (2)	2 (2)	4 (2)	3 (1)
RH	8 (7)	2 (1)	4 (1)	7 (5)	7 (1)	2 (0)
U	3 (2)	4 (1)	4 (3)	1 (0)	2 (1)	2 (2)
VPD	11 (9)	6 (2)	6 (2)	9 (7)	6 (2)	2 (0)
KBDI	6 (3)	8 (3)	6 (2)	6 (3)	8 (4)	8 (3)
PDSI	2 (1)	6 (2)	8 (5)	3 (2)	6 (4)	7 (3)
SPI	4 (4)	6 (3)	8 (4)	3 (2)	5 (3)	7 (2)

2.3. Correlation calculation and analysis

Denote a fire property as $F = F_t(i,j,k)$, where t is an indicator of time scale (length of time series element): t = month (m), season (s), or year (y); i a specific month of a year for $t = m$, a specific season of a year for $t = s$, or a constant value of 1 for t = y; $j = 1$, J (J = 21 is the number of years of the data series); $k = 1$, K (K = 28 is the number of provinces). Correspondingly, each meteorological variable or drought index is demoted as $M = M_t(i,j,k)$. The fire-meteorological correlation coefficient is denoted as $r_{F,M,t}(i,k)$.

We use $NC_{F,M,t}$ (i, σ) to denote the number of provinces with significant correlation at the level $\sigma = 0.1$, 0.05, or 0.01. Note that *NC* is not weighted using *F*. Thus, two variables with the same *NC* value but different provinces do not necessarily mean that they have the same level of close relationships with fires.

2.4. Prediction and fitting rate

Linear regression models were formed to predict F_t using M_t if $r_{F,M,t}(i,k)$ is significant:

$$F'_{M,t}(i,j,k) = a_t(i,k) + b_t(i,k) \times M_t(i,j,k) \quad (3)$$

where $F'_{M,t}(i,j,k)$ is predicted fire; $a_t(i,k)$ and $b_t(i,k)$ are intercept and slope, respectively.

The prediction results were analyzed in the following steps. (1) For each i and k, the $F_t(i,j,k)$ values ($j = 1$, J) were divided into three groups, above normal (the 7 largest *F values*), below normal (the 7 smallest values), and normal (the remaining 7 values). All $F'_{M,t}(i,j,k)$ values ($j = 1$, J) were divided into the three groups as well. (2) The fitting rate of the prediction of the above normal fires, $FR_{M,t}(i,k) = J'_{M,t}(i,k)/J \times 100\%$, was calculated, where $J'_{M,t}(i,k)$ is the number of years when both $F_t(i,j,k)$ and $F'_{M,t}(i,j,k)$ fall in the above normal group. (3) A meteorological variable / drought index (possibly more than one) with the maximum $FR_{M,t}(i,k)$ was determined. (4) The number of provinces with a fitting rate equal to or greater than a reference rate, FR_{ref}, was counted and denoted as NF_t (FR_{ref}) for the month with the largest monthly fire of a year ($t = m$), the season with the largest seasonal fire ($t = s$), and annual fire ($t = y$), respectively. The percentage, PNF_t (FR_{ref}) = NF_t (FR_{ref}) / K was calculated. FR_{ref} is either the random rate of 33% or a percentage used to indicate a high fitting rate.

3. Results

3.1. Fire properties

Annual *FC* and *FA* averaged over 1999–2019 varied remarkably across China (Fig. 2), both much larger in eastern than western China. The geographic distribution patterns in eastern China were opposite between *FC* and *FA*. Annual *FC* was much larger in southern than northern China. The value was 1200 in Hunan of SC and 1000 in Guizhou of SW, but only 80 in Daxing'anling of NE, which was about 6% of that in Hunan. In contrast, annual *FA* was larger in northern than southern China. The value was more than 60 k ha in Daxing'anling and 40 k ha in Heilongjiang of NE, but only 10 k ha in Yunnan of SW, which was 17% of that in Daxing'anling.

Forest fires in China occurred throughout the entire year (Fig. 3). Nationally, *FC* was the largest in spring (about 3800), followed by winter (2400), fall (500), and summer (300). *FC* in spring was larger in March (over 1800) and April (over 1700). *FC* values of winter, fall and summer were larger in February (1600), October (200), and June (120), respectively. Regional *FC* values were large in the southern regions of SC, SW, and CC, where monthly variations were similar to those of national *FC*.

Nationally, *FA* was also the largest in spring (over 140 k ha). However, the peak occurred in May instead of March for *FC*. The second largest *FA* of 35 k ha occurred in fall instead of winter for *FC*. *FA* was 24 and 13 k ha in winter and summer, respectively. The fall, winter, and summer peaks were 22 k ha in October, 16 in February, and 8 in June, respectively. NE had the largest *FA*, 3.5, 4.9 and 11.5 times of those in SC, SW and CC, despite only 12%, 18% and 23% of the *FC* values in these

regions.

The monthly variations showed another difference between southern and northern China. Southern China mainly had a single but long period of fire season from October to next April with the major fire activities from February to April in SC, and from late winter to early spring, especially from February to April, in SW and CC. In northern China, on the other hand, fire season had two periods in spring and fall in NE, and one short period in spring in NC.

The annual *FC* of China was nearly 15,000 in 2004 and 2008 (Fig. A1), with SC during winter 2004 and spring 2008 as the largest contributors. The *FC* in SW and CC also contributed. The year of 2004 was very dry in winter and slightly dry in spring in SC and CC, and warmer in winter and spring in CC (Fig. A2). The year of 2008 was dry in winter in CC and in spring in SW, and warm in spring in SW and CC. Annual *FA* was about 1100 k ha in 2003 and 600 k ha in 2006 (Fig. A1), with NE during springs of the two years as dominant contributors. It was dry and / or warm in springs of both years (Fig. A2).

3.2. Number of provinces with significant fire-meteorological correlations

NC_t (*F, M, σ*), the number of provinces with significant fire-meteorological correlation $r_{F,M,t}(i,k)$ at the level σ, is shown in Fig. 4. NC_m (*F, M, σ*) is the average of three consecutive months with the middle month having the largest fire of a year. NC_s (*F, M, σ*) is the value for the season with the largest fire of a year. Note that $r_{F,M,t}(i,k)$ is normally positive for $M = T_{max}$, *U*, *VPD*, and *KBDI*, and negative for $M = R$, *RH*, *PDSI*, and *SPI*. However, there might be cases of opposite signs for one or more provinces. These cases were not counted in NC_t (*F, M, σ*).

NC_m (*FC, M, 0.1*) (Fig. 4a) is 15–17 for $M = RH$, *VPD*, and *KBDI*, 13 for $M = T_{max}$, and below 10 for *R, U, PDSI,* and *SPI*. NC_m (*FC, M, 0.05*) and NC_m (*FC, M, 0.01*) are also larger for *RH, VPD*, and *KBDI* but the values are reduced by approximately 5 for $\sigma = 0.05$ and 10 for $\sigma = 0.01$ from those for $\sigma = 0.1$. NC_s (*FC, M, 0.1*) (Fig. 4b) remains more than 15 for KBDI, but is reduced to 11 for *RH* and *VPD*, and to 5 for T_{max}. The number is 10–11 for *PDSI* and *SPI*. N_y (*FC, M, 0.1*) (Fig. 4c) is 13–14 for *KBDI* and *PDSI*, 10 for *SPI*, but 8 or smaller for all meteorological variables.

NC_t (*FA, M, σ*) is generally similar to NC_t (*FC, M, σ*). NC_m(*FA, M, 0.1*) is greater than 14 for *RH* and *VPD* and 12 for *KBDI*, though NC_m(*FA, M, 0.05*) is greater than 10 for *VPD* and *KBDI*. N_s(*FA, M, 0.1*) is greater than 15 for *RH*, 13 for *KBDI*, and 11 for *VPD* and *PDSI*.

The result indicates that *RH, VPD*, *KBDI*, and *PDSI* are often significantly correlated with fires in more provinces than other meteorological variables and drought indices. The number of provinces was the largest for *RH* and *VPD* at monthly scale and for *KBDI* and *PDSI* at seasonal and annual scales.

3.3. Spatial patterns of fire-meteorological correlations

The provinces with significant $r_{F,M,t}(i,k)$ ($p < 0.1$ or a higher level, same hereafter) are displayed in Figs. 5-8. Here $t = m$ is the month of a year with the largest monthly *F*. Note that this is different from Fig. 4 in which the monthly values are averaged over three months rather than one month. Similarly, $t = s$ is the season of a year with the largest seasonal *F*.

The provinces with significant $r_{FC,\ Tmax,m}$ (i,k) are found mainly in NE and SW (Fig. 5), two of the major fire regions in China. The number of provinces in SW with significant $r_{FC,\ Tmax,s}$ (i,k) or $r_{FC,\ Tmax,y}$ (i,k) is reduced. The provinces with significant $r_{F,R,t}$ (i,k) are also found in SC (Fig. 6). Many provinces with significant $r_{F,VPD,t}$ (i,k) are found not only in NE and SW but also NC, CC, SC, and NW (Fig. 7). However, almost no provinces are found in SW for $t = s$ and $t = y$. The provinces with significant $r_{F,KBDI,t}$ (i,k) are found mainly in NE, CC, SC, and SW (Fig. 8). However, no provinces are found in NE for *FA*. The result indicates a common feature of significant correlations in NE and SW for all the four meteorological variables and drought indices and a different feature of significant correlations in some other regions as well for *VPD* and *KBDI*.

3.4. Seasonal dependence of fire-meteorological correlations

As shown in Fig. 3, *FC* and *FA* in all the major fire regions (NE, NC, CC, SC, and SW) were the largest in spring. The number of provinces with significant $r_{FC,KBDI,s}(i,k)$ during spring (Fig. 9b) is larger than or comparable to that during other seasons (Fig. 9a, c-d). This seasonal difference is seen for the number of provinces with significant $r_{FA,KBDI,s}(i,k)$ as well except that the number of provinces in NE is smaller during spring (Fig. 9f) than summer and fall (Fig. 9g-h). However, the number of provinces with significant $r_{F,M,s}(i,k)$ is smaller during spring than some other seasons for most meteorological variables. The number of provinces with significant $r_{F,Tmax,s}(i,k)$ is 5 for *FC* and 2 for *FA* during spring, which are only about half of the numbers during other seasons (Fig. A3). The number of provinces with significant $r_{F,M,s}(i,k)$ during spring is also smaller than that during fall for *R* (Fig. A4), and during winter and fall for *VPD* (Fig. A5).

3.5. Prediction fitting rate

The highest fire prediction fitting rate among all meteorological variables and drought indices, $FR_{M,t}(k)$, is listed in Table A1 for *FC*. The number of provinces where fitting rate is larger than the random rate of 33%, NF_t (33%), is 25, 23, and 21 for $t = m$, *s,* and *y*, respectively (Table 2). The corresponding percentage, PNF_t (33%), is 89, 82, and 75. Regionally, except for TI, the percentage in other regions is more than 80, 60, and 50 for $t = m$, *s*, and *y*, respectively. For a high fitting rate of 71% or better, NF_t (71%) is 18, 12, and 10 for $t = m$, *s,* and *y*, respectively. The corresponding PNF_t (71%) is 64, 43, and 36. The percentage is 50 or above in NE and CC at all time scales, SC for $t = m$ and *s*, and NC and SW for $t = m$.

NF is classified into high, average, and small for $NF \geq 9$, 5–8, and ≤ 4, respectively. The meteorological variables and drough indices in the high class are more important fire predictors. NF_m (33%) is high for *VPD*, average for T_{max}, *RH*, and *KBDI*, and small for others (Table 3). NF_s (33%) and NF_y (33%) are average for *KBDI*, *VPD*, *PDSI*, and *SPI*, and small for others. NF_m (71%) is high for *VPD*, average for T_{max} and *RH*, and small for others. NF_s (71%) is small for all variables and indices. NF_y (71%) is average for *PDSI* and small for others. The result indicates that the most important predictors in terms of the number of provinces with the largest fitting rates are *VPD* for monthly *FC*, *KBDI* for seasonal *FC*, and *PDSI* and *SPI* for annual *FC*. The important predictors also include T_{max}, *RH*, and *KBDI* for monthly *FC*, *VPD*, *PDSI*, and *SPI* for seasonal *FC*, and *VPD* and *KBDI* for annual *FC*.

$FR_{M,t}(k)$ for *FA* is listed in Table S2. NF_t (33%) (Table 2) is generally similar to that for *FC* but with a couple of differences. First, NF_m (33%) and PNF_t (33%) are smaller, 20 (71%) for *FA* vs. 25 (89%) for *FC*. So are NF_m (71%) and PNF_t (71%), with 13 (46%) for *FA* vs. 18 (64%) for *FC*. Secondly, *KBDI* becomes the most important predictor instead of *PDSI* and *SPI* ($t = y$).

4. Discussion

The results described above indicate that *VPD* and *RH* have significant correlations with long-range fires and high fitting rates in more provinces than T_{max} and *R*, while *KBDI* and other drought indices often have significant correlations and high fitting rates for seasonal and annual fires in more provinces than all meteorological variables. Fire occurrence and spread are determined by both atmospheric thermal and hydrological conditions. Unlike temperature, which only measures atmospheric thermal condition, *VPD* and *RH* measure both atmospheric thermal and hydrological conditions. *VPD* is more dynamical than *RH* (Sedano and Randerson, 2014; Seager et al., 2015). The evidence for high skills of operational seasonal forecasts of burned area using *SPI* was provided recently (Turco et al. 2018). Unlike *VPD* and other

meteorological variables that measure atmospheric thermal and hydrological conditions, *KBDI* and other drought indices are determined by soil water anomalies. According to the air-land interaction studies, soil hydrological processes in the local atmosphere-soil-vegetation system have much longer scales than atmospheric processes (Liu and Avissar, 1999). Another difference is that, *KBDI* of a day depends on the value on a prior day. Thus, it is an accumulated property which can better reflect anomalies over a long time.

The fire-meteorological relationships show strong geographic dependence. NE, CC, and SC have the highest percentage of provinces with significant fire correlations and prediction fitting rates. These regions are among the main fire regions of China and located mainly in the relative flat Step 1 of topography. TI and NW have the lowest percentage, the two regions with very small fire number and burned area and located in the complex Step 3 of topography. SW and NC has high percentage for monthly and / or seasonal fires. The regional dependence suggests the fire-meteorological relationships are determined by both fire activity and topography.

The number of provinces with significant fire-meteorological correlations is often smaller in spring, the season with the largest fires, than some other seasons for meteorological variables. Spring is a transition season from winter to summer monsoon phase. Meteorological conditions in spring are extremely dynamic and variable. This is probably a reason for the relatively poor fire-meteorological relationships. However, the seasonal dependence is not visible for *KBDI*. As an accumulated property, *KBDI* is determined not only by the meteorological conditions of the current season but also prior seasons, which reduces the impact of the highly varied meteorological conditions during spring.

The fire correlations and prediction fitting rates are generally smaller for burned areas than fire count. This feature may be related to the fire management policy in China. Forest coverage in China is 23%, only about half of that in the United States despite comparable land area. The strict fire prevention and suppression strategies adopted after the catastrophic 1987 Daxing'anling fires to preserve forest resources limit fire spread although more fires could occur under droughts and other abnormal weather and fuel conditions (Guo et al. 2015). Thus, burned areas may not necessarily increase accordingly, leading to the weaker meteorological relationships.

Understanding of the underlying meteorological/climatic forcing factors for the fire-meteorological relationships is valuable for predictions of regional fires in China. To discuss this issue, we analyzed the differences in the 500 hPa geopotential heights over Eurasia between the five years with the largest and smallest fires for each of the five major fire regions. The fires of the five years were approximately in the 75th and 25th percentile of fires of all years, respectively. The averaged 500 hPa geopotential heights were controlled by three circulation systems (Fig. A6): the polar vortex with low pressure in the high latitudes; the westerly streams in the middle latitudes, with the western Mongolia ridge from western China to Siberia, and the East Asian trough from northeastern China to the Russian Far East; and the subtropical highs in the low latitudes over the Northwest Pacific Ocean and northeastern Africa.

For fire counts (Fig. A7), the spatial patterns of the differences are similar between NE and SC, which are mainly negatively in the high latitudes but positive in the middle latitudes. The positive differences are especially strong over NE at monthly and seasonal scales. Fire counts at yearly scale in SC are also affected by the circulations in the low latitudes. The result suggests that stronger polar vortex and weaker East Asian trough / stronger western Mongolia ridge are the major atmospheric circulation drivers for larger fire counts. The patterns for fire counts in NC and CC are opposite to those in NE and SC. The differences for SW are negative in the polar vortex area at yearly scale, but spilt between positive in the west and negative in the east at monthly and seasonal scales. For burned areas (Fig. A8), the spatial patterns of the differences are similar between monthly and seasonal scales but substantially different for yearly scale. The patterns are more or less similar to those of fire counts in NE, NC, and CC. The circulations in the low latitudes are related more closely to burned areas than fire counts at seasonal and yearly scales. Further research is needed to understand the physical mechanisms for the atmospheric drivers and the complex relationships of the drivers with fire regions, time scales, and properties.

An urgent issue in fire research and management in China is how to project future fires under the changing climate and develop mitigation strategies (Liu et al. 2012; Tian et al. 2014, 2017). Same as fire predictions, meteorological variables such as temperature and precipitation (including fire danger rating obtained based on these variables) are often used to project future fires. The results from this study suggest that, for the future trends in statistics of fires (monthly, seasonal, and annual averages) rather than individual fires, other meteorological variables such as VPD and drought indices such as KBDI might be more appropriate indicators for future fire trends.

5. Conclusions

Currently, temperature and precipitation are the primary meteorological predictors for operational monthly and seasonal fires in the individual provinces of China. It was found from this study that vapor pressure deficit and relative humidity have significant correlations with long-range fire count and burned area and the prediction fitting rates larger than the random rate in more provinces than temperature and precipitation, while *KBDI* and other drought indices often have significant correlations and high fitting rates for seasonal and annual fires in more provinces than all meteorological variables. In addition, the number of provinces with significant fire correlations is often smaller during the major fire season of spring than some other seasons for meteorological variables but not for *KBDI*. It is concluded based on these findings that vapor pressure deficit is the most important meteorological predictor for monthly provincial fires in China and *KBDI* for seasonal and annual fires. The prediction skills of long-range fires are expected to be improved in many provinces of China by including vapor pressure deficit and *KBDI* as well as some other meteorological variables and other drought indices as predictors.

Declaration of Competing Interest

The authors declare that they have no known competing financial interests or personal relationships that could have appeared to influence the work reported in this paper.

Acknowledgements

This study was supported by the USDA Forest Service, China National Key Research and Development Plan (2020YFC1511601), and China Natural Science Foundation under project (32071778). We appreciate the constructive and detailed review comments for improving this manuscript, and thank Shela Mou for English edits. The elevation and land cover information were obtained from International Steering Committee for Global Mapping (ISCGM). The authors do not have a conflict of interest.

Appendix

See Figs. A1-A8.
See Tables A1-A2.

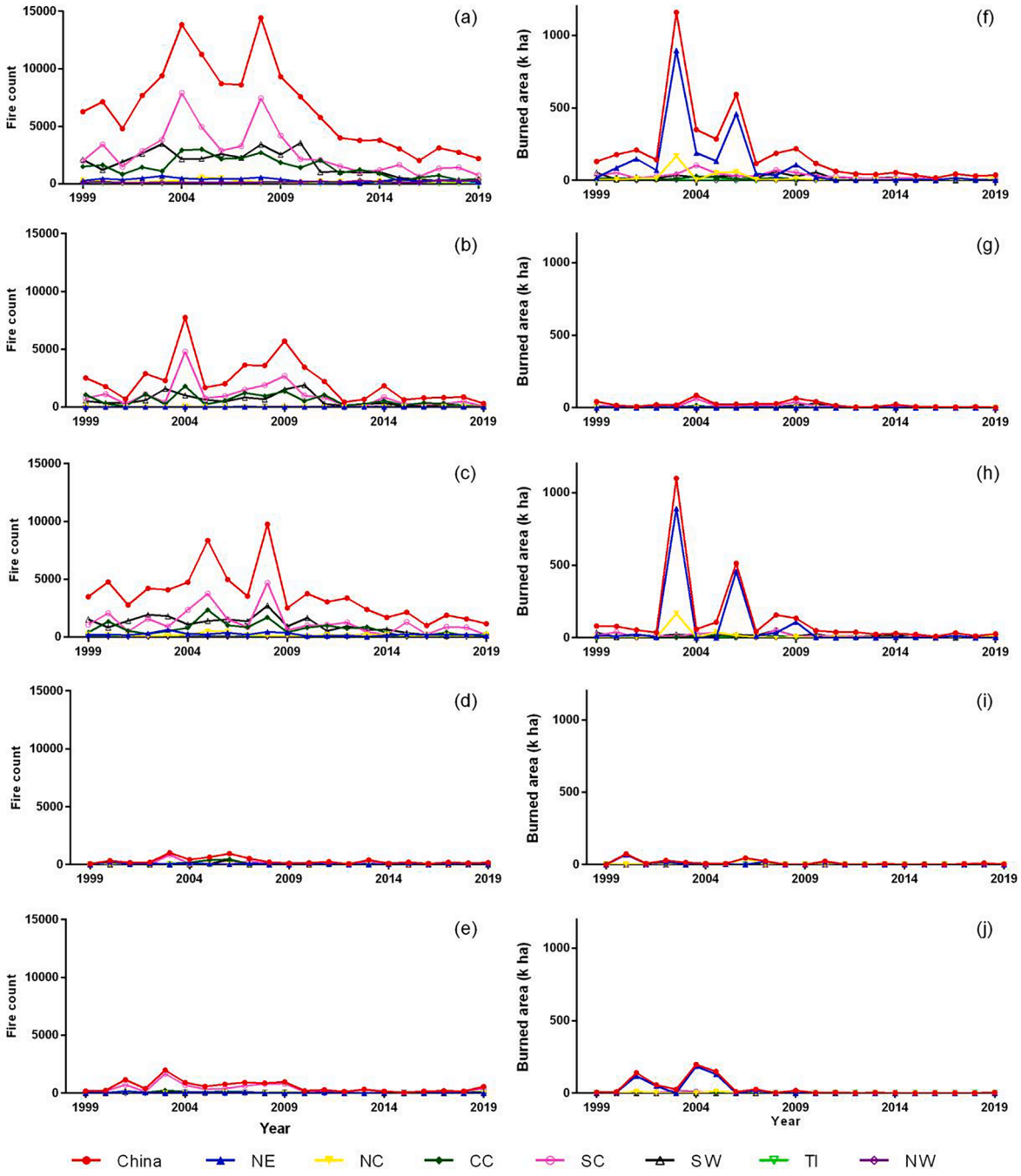

Fig. A1. Inter-annual variability of annual and seasonal fire count and burned area for 1999–2017. The eight lines in each panel represent China and seven regions. The panels are fire count (a-e) and burned area (f-j) of year, winter, spring, summer, and fall. (see Table 1 and Fig. 2 for the full names and locations of these regions.)

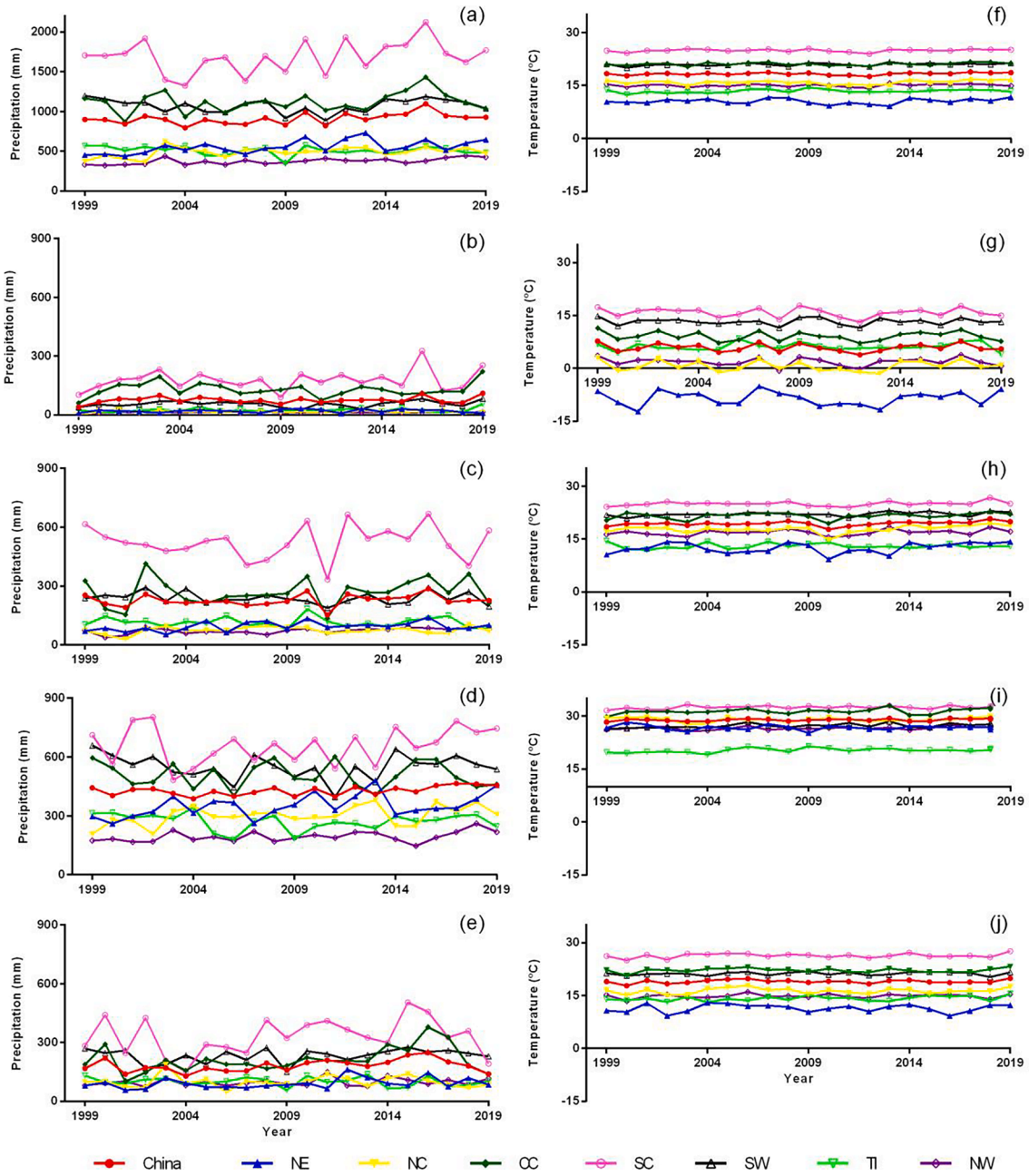

Fig. A2. Annual and seasonal precipitation and temperature in China and different regions during 1999–2017. The eight lines in each panel represent China and seven regions. The panels are precipitation (a-e) and temperature (f-j) of year, winter, spring, summer, and fall. (see Table 1 and Fig. 2 for the full names and locations of these regions.)

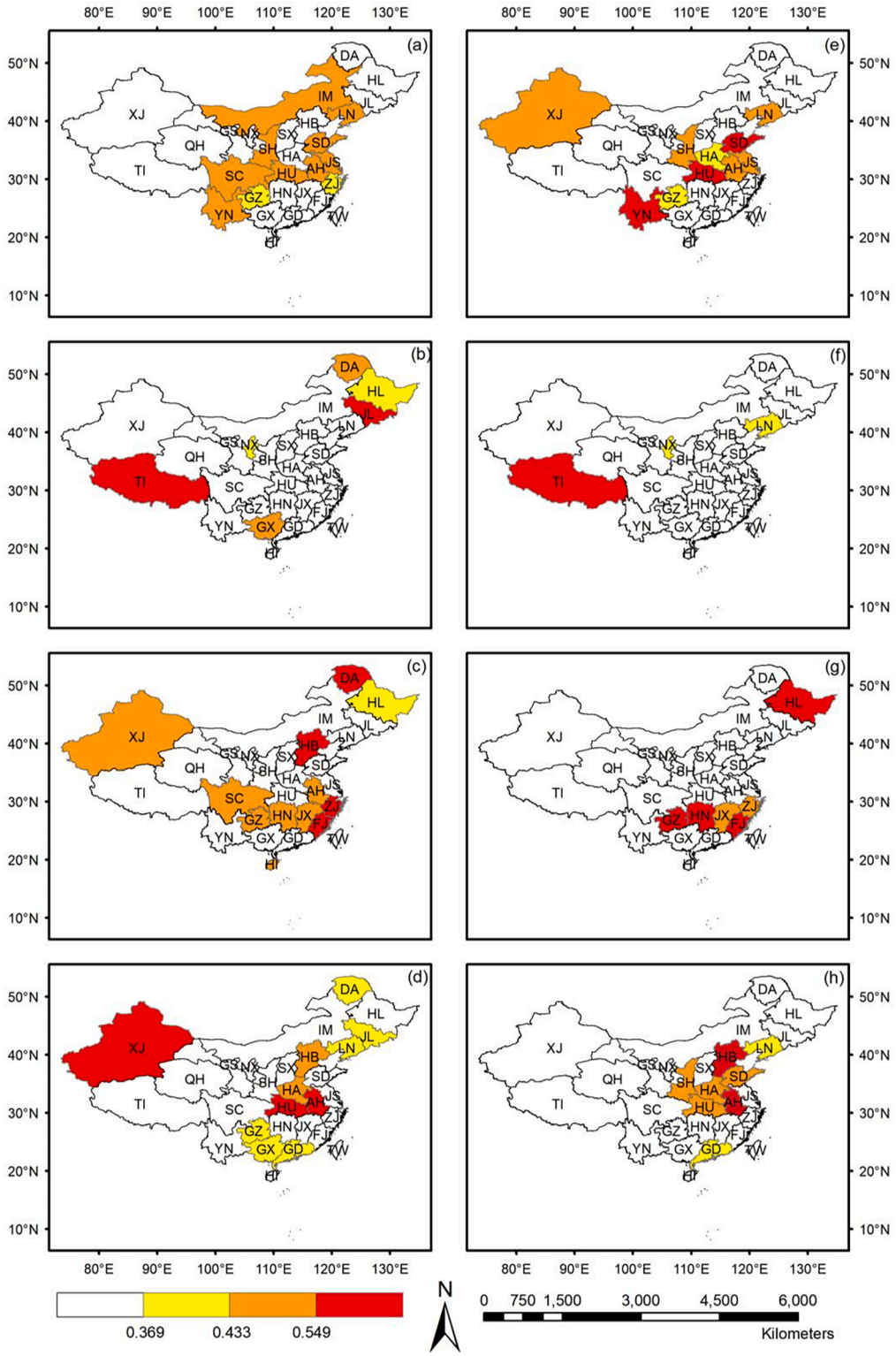

Fig. A3. Provinces with significant seasonal fire-maximum temperature correlations. (a-d) are for winter, spring, summer, and fall of fire count. (e-h) are the corresponding burned area. The critical values are 0.369 ($p < 0.1$), 0.433 ($p < 0.05$), and 0.549 ($p < 0.01$).

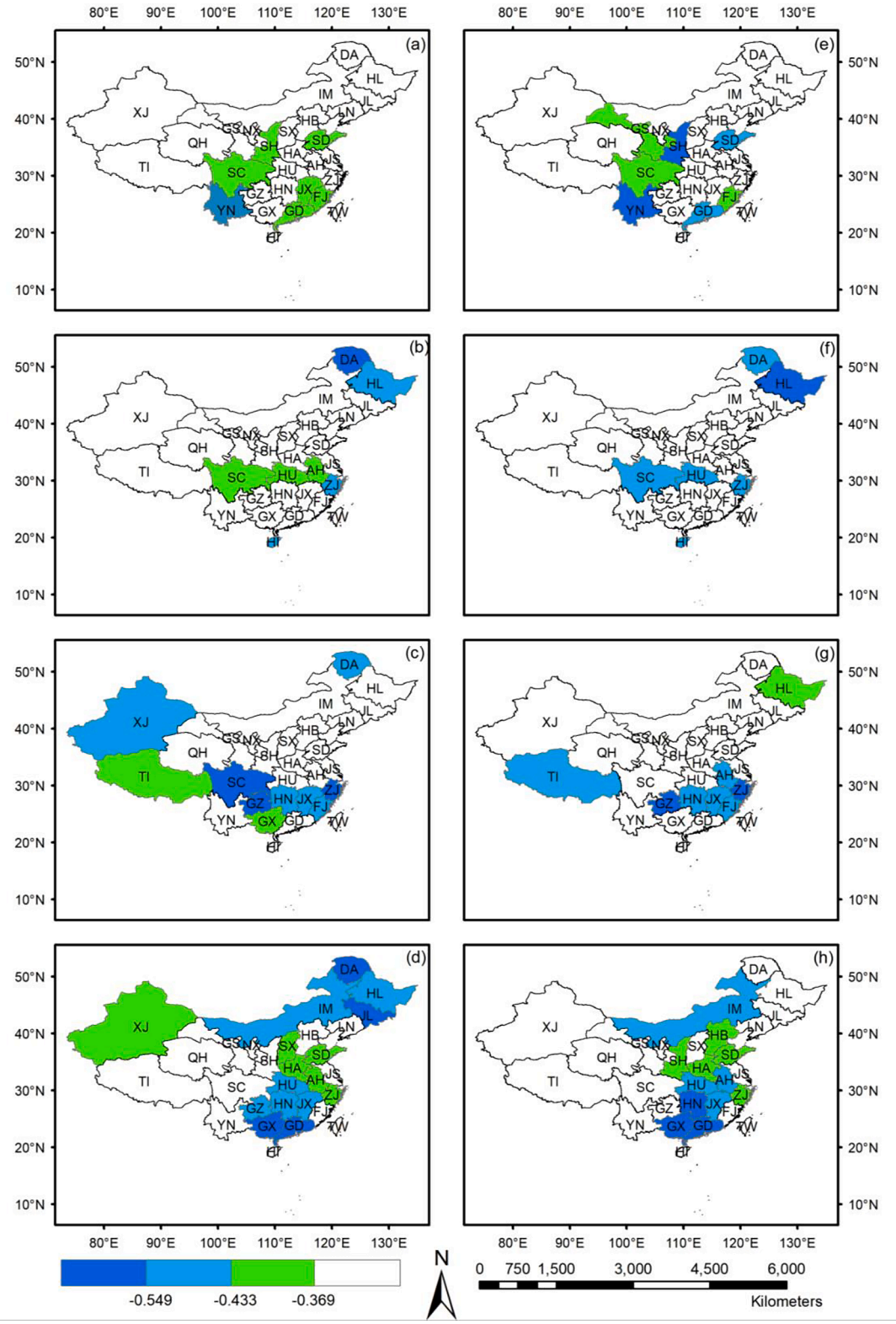

Fig. A4. Provinces with significant seasonal fire-precipitation correlations. (a-d) are for winter, spring, summer, and fall of fire count. (e-h) are the corresponding burned area. The critical values are 0.369 ($p < 0.1$), 0.433 ($p < 0.05$), and 0.549 ($p < 0.01$).

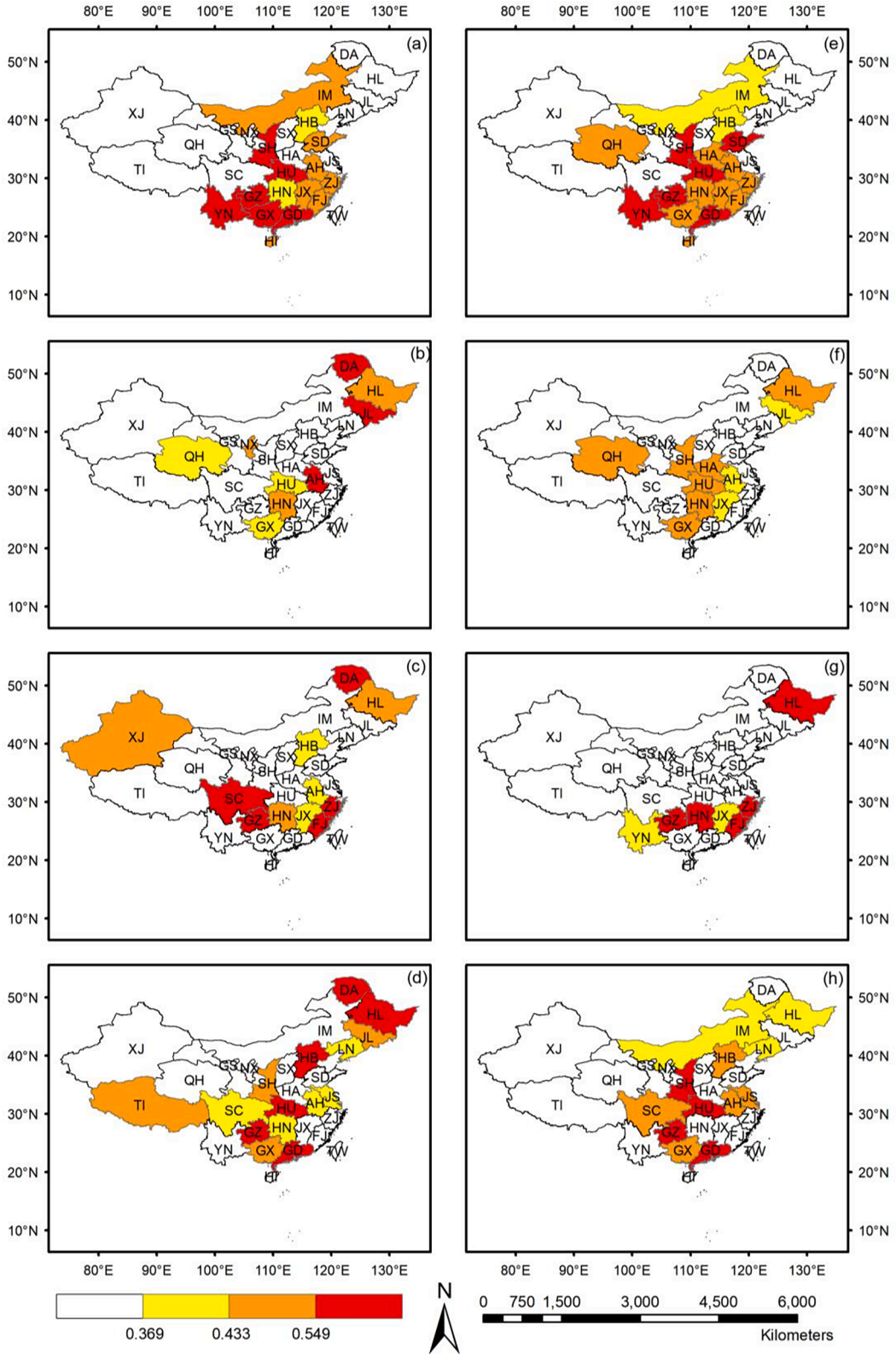

Fig. A5. Provinces with significant seasonal fire-vapor pressure deficit correlations. (a-d) are for winter, spring, summer, and fall of fire count. (e-h) are the corresponding burned area. The critical values are 0.369 ($p < 0.1$), 0.433 ($p < 0.05$), and 0.549 ($p < 0.01$).

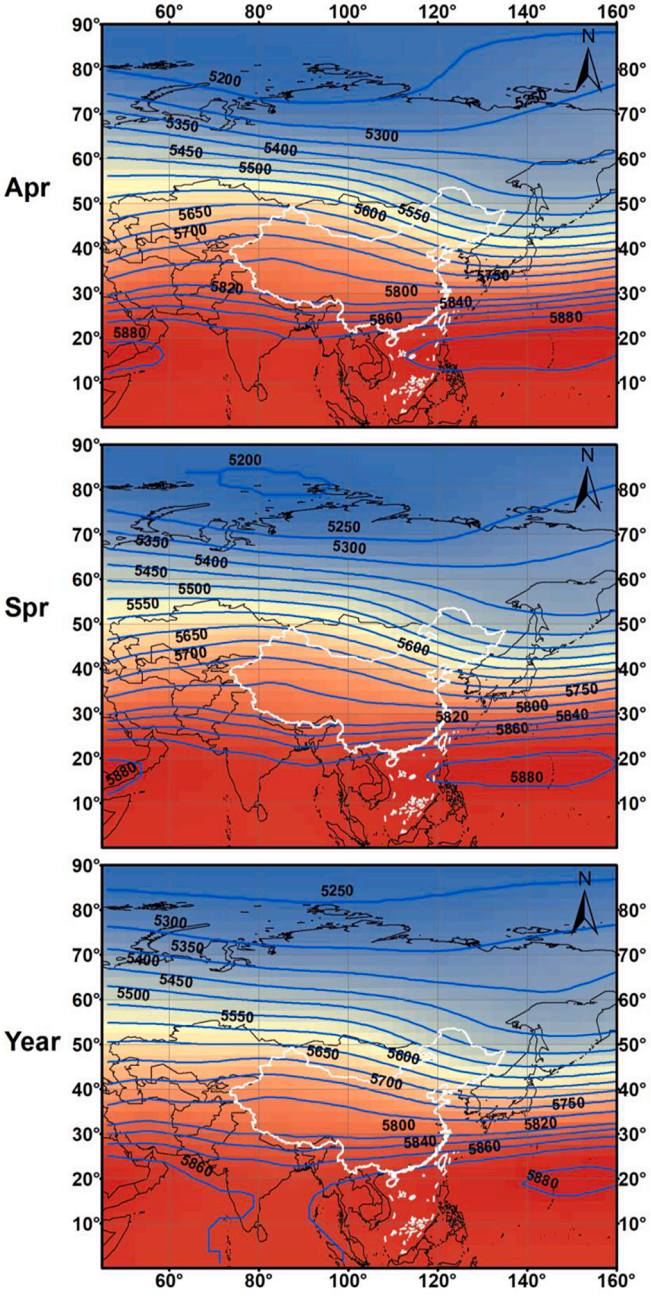

Fig. A6. 500 hPa geopotential height (m). From top to bottom are for April, spring, and year.

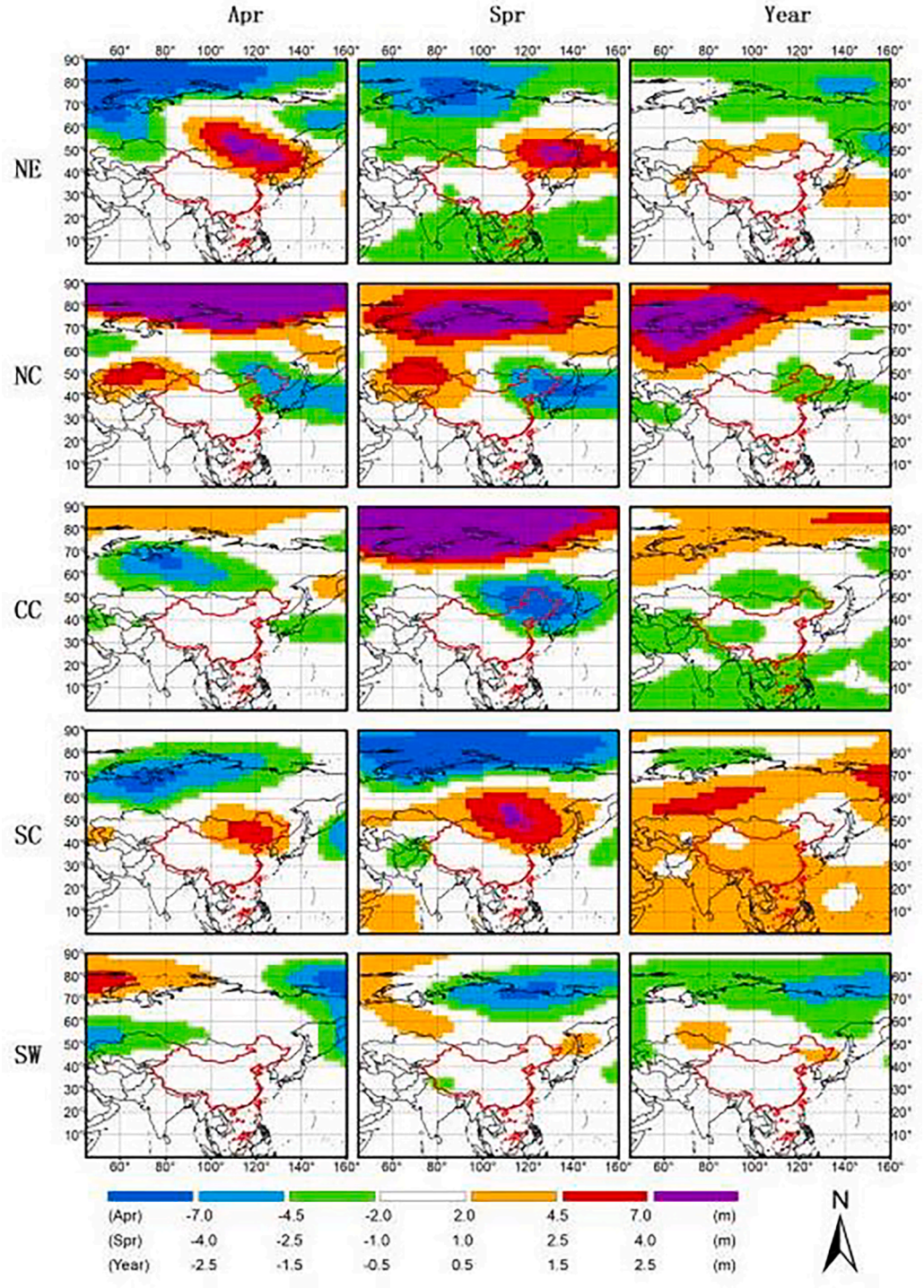

Fig. A7. Differences in 500 hPa geopotential height (m) between the five years with the highest fire counts and the five years with the lowest ones. From left to right are for April, spring, and year. From top to bottom are for Northeast, North, Central, South, and Southwest China.

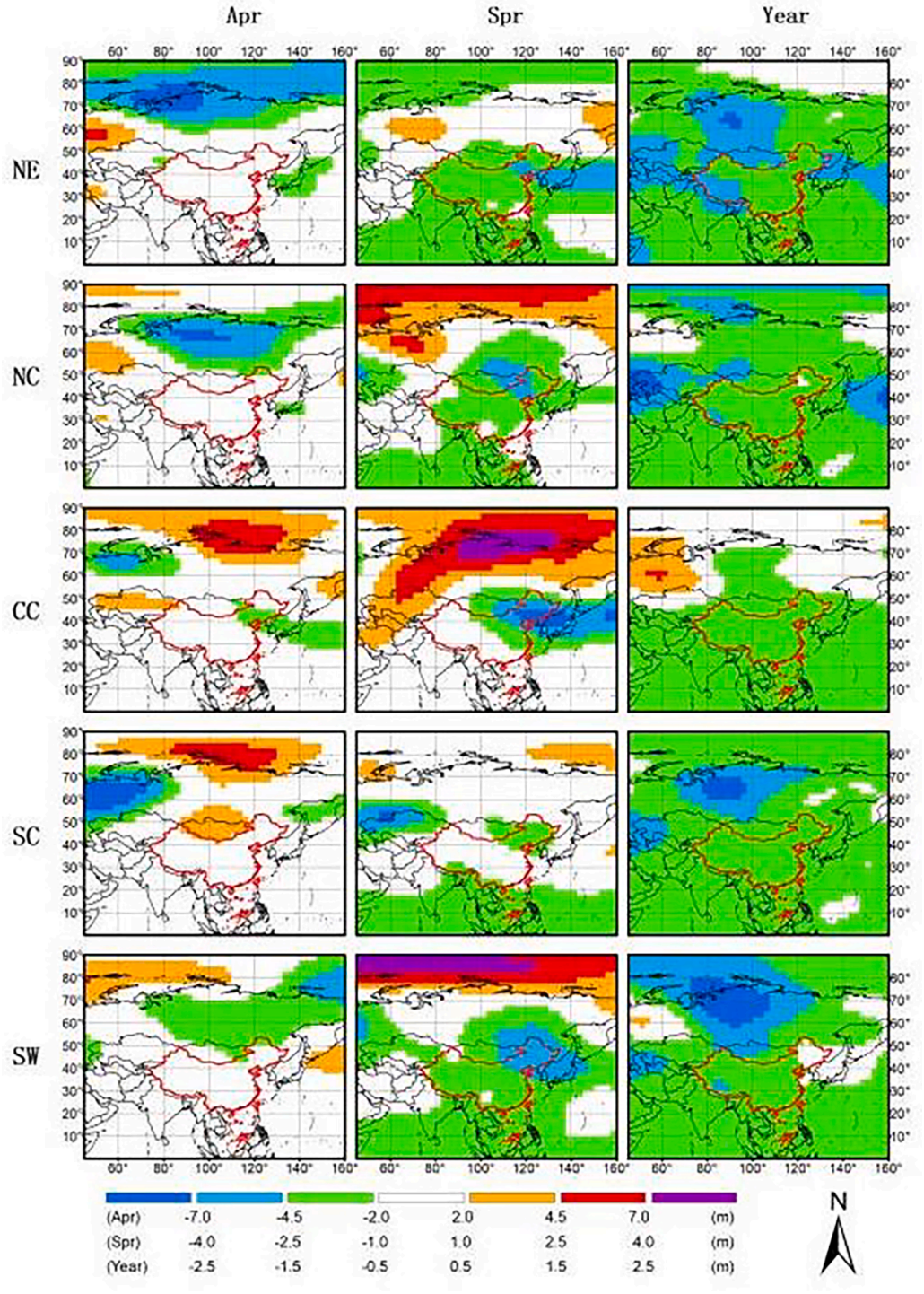

Fig. A8. Differences in 500 hPa geopotential height (m) between the five years with the largest burned areas and the five years with the smallest ones. From left to right are for April, spring, and year. From top to bottom are for Northeast, North, Central, South, and Southwest China.

Table A1
Prediction fitting rates (%) of above normal provincial fire count. The variable is meteorological variable (s) / drought index (indices) used as a predictor. x and y indicate no significant correlation between fire count and a meteorological variable / drought index and a fitting rate lower than the random rate of 33%.

Region	Province	Monthly		Seasonal		Annual	
		Rate	Variable	Rate	Variable	Rate	Variable
NE	DA	85	RH	71	KBDI	71	T_{max}
	HL	57	T_{max},KBDI,PDSI	71	PDSI	71	R,U,VPD,PDSI,SPI
	JL	85	VPD	71	VPD	42	T_{max},VPD
	LN	57	T_{max}	57	KBDI	x	
NC	IM	71	T_{max},RH,VPD	x		x	
	HB	71	SPI	42	RH,U	x	
	SX	57	KBDI	57	KBDI	57	RH,VPD,KBDI,SPI
	SD	71	U	85	U	71	U
CC	HA	71	RH	57	PDSI, SPI	71	PDSI
	AH	85	T_{max}, VPD	71	RH,PDSI	71	PDSI
	HU	42	RH	71	VPD	57	RH
	JS	x		57	U,KBDI	71	U
	ZJ	85	R,RH,SPI	85	R	71	SPI
SC	HN	71	VPD,PDSI	57	VPD,PDSI	85	PDSI
	JX	71	RH,VPD	71	SPI	57	KBDI,PDSI,SPI
	FJ	71	T_{max}, VPD	71	KBDI	57	R, KBDI,PDSI, SPI
	GD	71	KBDI	85	SPI	57	R,SPI
	GX	71	RH,KBDI	42	T_{max},VPD	57	KBDI
	HI	57	U,KBDI	57	R,U,KBDI,PDSI,SPI	71	R,KBDI,SPI
SW	SC	71	T_{max}, R, VPD	57	R,KBDI,PDSI,SPI	71	RH,VPD,KBDI,PDSI,SPI
	GZ	71	T_{max}	71	KBDI	57	RH,PDSI
	YN	71	VPD,KBDI,SPI	x		y	
TI	TI	x		x		x	
NW	SH	71	R,RH,VPD,SPI	x		x	
	GS	x		71	SPI	x	
	QH	71	U	57	VPD	57	U
	NX	57	VPD	57	VPD	57	VPD
	XJ	57	VPD	x		57	VPD

Table A2
Prediction fitting rates (%) of above normal provincial burned area. The variable is meteorological variable (s) / drought index (indices) used as a predictor. x and y indicate no significant correlation between fire count and a meteorological variable / drought index and a fitting rate lower than the random rate of 33%.

Region	Province	Monthly		Seasonal		Annual	
		Rate	Variable	Rate	Variable	Rate	Variable
NE	DA	57	T_{max}, KBDI,PDSI	71	PDSI	x	
	HL	57	T_{max}	71	R,PDSI	71	PDSI
	JL	x		57	VPD	42	R,SPI
	LN	57	T_{max}	71	T_{max}	42	T_{max}
NC	IM	x		x		x	
	HB	57	U	57	RH	42	RH
	SX	x		57	RH,VPD	57	RH,VPD, SPI
	SD	71	R,SPI	42	RH	x	
CC	HA	71	RH	57	RH,VPD	57	PDSI, SPI
	AH	71	T_{max},VPD	57	R,RH,KBDI,PDSI	71	PDSI
	HU	71	T_{max},VPD,KBDI	85	VPD	57	KBDI
	JS	x		57	KBDI,PDSI	71	U
	ZJ	71	R,RH,PDSI,SPI	71	R,KBDI,PDSI,SPI	71	SPI
SC	HN	71	VPD,PDSI	71	RH,VPD,KBDI,PDSI	85	PDSI
	JX	71	T_{max}	71	KBDI	57	KBDI,PDSI,SPI
	FJ	71	T_{max},VPD	71	KBDI	57	R, KBDI, PDSI, SPI
	GD	71	RH,VPD	85	SPI	71	KBDI
	GX	85	VPD	85	SPI	85	KBDI,PDSI
	HI	x		57	U	71	R
SW	SC	57	KBDI,SPI	57	R,KBDI,SPI	71	SPI
	GZ	42	RH,VPD,KBDI	x		57	KBDI
	YN	85	RH,VPD,KBDI	42	KBDI,SPI	42	KBDI
TI	TI	x		x		x	
NW	SH	71	KBDI	71	U	71	KBDI
	GS	x		x		x	
	QH	71	RH	57	RH,VPD	71	U
	NX	42	RH,VPD	42	T_{max}	57	VPD
	XJ	x		x		x	

References

Abatzoglou, J.T., Kolden, C.A., 2013. Relationships between climate and macroscale area burned in the western United States. Int. J. Wildlandfire 22 (7), 1003–1020.

Abatzoglou, J.T., Williams, A.P., 2016. Impact of anthropogenic climate change on wildfire across western US forests. Proc. Natl. Acad. Sci. 113, 11770–11775.

Assal, T.J., Anderson, P.J., Sibold, J., 2016. Spatial and temporal trends of drought effects in a heterogeneous semi-arid forest ecosystem. For. Ecol. Manage. 365, 137–151.

Bedia, J., Golding, N., Casanueva, A., Iturbide, M., Buontempo, C., Gutiérrez, J.M., 2018. Seasonal predictions of Fire Weather Index: Paving the way for their operational applicability in Mediterranean Europe. Cliamte Services 9, 101–110.

Bo, M., Mercalli, L., Pognant, F., Berro, D.C., Clerico, M., 2020. Urban air pollution, climate change and wildfires: The case study of an extended forest fire episode in northern Italy favoured by drought and warm weather conditions. Energy Rep. 6, 781–786.

Brown, T., Leach, S., Wachter, B., Gardunio, B., 2020. The Extreme 2018 Northern California Fire Season. Bull. Am. Meteorol. Soc. 101, S1–S4.

Cahoon, D.R., Stocks, B.J., Levine, J.S., Cofer, III W.R., Pierson, J.M., 1994. Satellite analysis of the severe 1987 forest fires in northern China and southeastern Siberia. J. Geophys. Res., 99(D9), 18627-18638.

Chen, D.M., Pereira, J.M.C., Masiero, A., Pirotti, F., 2017. Mapping fire regimes in China using MODIS active fire and burned area data. Appl. Geogr. 85, 14–26.

Chen, Y., Randerson, J.T., Morton, D.C., DeFries, R.S., Collatz, G.J., Kasibhatla, P.S., Giglio, L., Jin, Y.F., Marlier, M.E., 2011. Forecasting fire season severity in South America using sea surface temperature anomalies. Science 334, 787–791.

Dai, A.G., 2011. Characteristics and trends in various forms of the Palmer Drought Severity Index during 1900–2008. J. Geophys. Res. 116, D12115.

Deeming, J.E., Burgan, R.E., Cohen, J.D., 1977. The National Fire-Danger Rating System – 1978. USDA Forest Service, Intermountain Forest and Range Experiment Station, General Technical Report INT-39, Ogden, Utah. 63 pp.

Doerr, S., Santín, C., 2016. Global trends in wildfire and its impacts: perception versus realities in a changing world. Philosophical Trans. Roy. Soc. B 371, 20150345.

Dowdy, A.J., Mills, G.A., 2012. Atmospheric and fuel moisture characteristics associated with lightning-attributed fires. J. Appl. Meteorol. Climatol. 51, 2025–2037.

Drobyshev, I., Niklasson, M., Linderholm, H.W., 2012. Forest fire activity in Sweden: Climatic controls and geographical patterns in 20th century. Agric. For. Meteorol. 154–155, 174–186.

Du, J.Z., Wang, K., Cui, B.S., 2021. Attribution of the Extreme Drought-Related Risk of Wildfires in Spring 2019 over Southwest China. Bull. Am. Meteorol. Soc. S83–S90.

Fang, K.Y., Yao, Q.C., Guo, Z.T., Zheng, B., Du, J.H., Qi, F.Z., Yan, P., Li, J., Ou, T.H., Liu, J., He, M.S., Trouet, V., 2021. ENSO modulates wildfire activity in China. Nat. Commun. 12, 1764.

Flannigan, M.D., Krawchuk, M.A., de Groot, W.J., Wotton, M., Gowman, L.M., 2009. Implications of changing climate for global wildland fire. Int. J. Wildland Fire 9 (18), 483–507.

FRC (Forest Resources in China), 2014. The 8th National Forest Inventory. State Forestry Administration, P.R. China. February, 2014. http://www.forestry.gov.cn/gjslzyqc.ht.

Gill, A.M., Stephens, S.L., 2009. Scientific and social challenges for the management of fire-prone wildland–urban interfaces. Environ. Res. Lett. 034014.

Goodrick, S.L., Brown, T.J., Jolly, W.M., 2017. Weather, fuels, fire behavior, plumes, and smoke - the nexus of fire meteorology. Fire Manage. Today 75 (1), 33–38.

Goodrick, S.L., Hanley, D.E., 2009. Florida wildfire activity and atmospheric teleconnections. Int. J. Wildland Fire 18, 476–482.

Gudmundsson, L., Rego, F.C., Rocha, M., Seneviratne, S.I., 2014. Predicting above normal wildfire activity in southern Europe as a function of meteorological drought. Environ. Res. Lett. 9, 084008.

Guo, F.T., Innes, J.L., Wang, G., Ma, X., Sun, L., Hu, H., Su, Z., 2015. Historic distribution and driving factors of human-caused fires in the Chinese boreal forest between 1972 and 2005. J. Plant Ecol. 8 (5), 480–490.

Guo, F.T., Wang, G.Y., Su, Z.W., Liang, H.L., Wang, W.H., Lin, F.F., Liu, A.Q., 2016. What drives forest fire in Fujian, China? Evidence from logistic regression and Random Forests. Int. J. Wildland Fire 25, 505–519.

Holdena, Z.A., Swansonb, A., Lucec, C.H., Jollyd, W.M., Manetae, M., Oylerf, J.W., Warrenb, D.A., Parsonsd, R., Affleckg, D., 2018. Decreasing fire season precipitation increased recent western US forest wildfire activity. Proc. Nat. Acad. Sci. USA 1802316115.

Jia, B.R., Zhou, G.S., Yu, W.Y., Fang, D.M., 2011. Characteristics of lightning fire in Daxing'anling Forest Region from 1972 to 2005 and its relationships with drought index. Scientia Silvae Sinicae 47 (11), 99–105.

Keetch, J.J., Byram, G.M., 1968. A drought index for forest fire control. USDA Forest Service Research Paper SE-38 (revised 1988). Asheville, NC.

Koutsias, N., Xanthopoulos, G., Founda, D., Xystrakis, F., Nioti, F., Pleniou, M., Mallinis, G., Arianoutsou, M., 2013. On the relationships between forest fires and weather conditions in Greece from long-term national observations (1894–2010). Int. J. Wildland Fire 2, 493–507.

Li, J.F., Song, Y., Huang, X., Li, M.M., 2015. Comparison of forest burned areas in mainland China derived from MCD45A1 and data recorded in yearbooks from 2001 to 2011. Int. J. Wildland Fire 24, 103–113.

Li, X.W., Zhao, G., Yu, X.B., Yu, Q., 2013. A comparison of forest fire indices for predicting fire risk in contrasting climates in China. Nat. Hazards. https://doi.org/10.1007/s11069-013-0877-6.

Lima, C.H., AghaKouchak, A., Randerson, J.T., 2018. Unraveling the role of temperature and rainfall on active fires in the Brazilian Amazon using a nonlinear Poisson model. J. Geophys. Res.-Biogeosci. 123, 117–128.

Littell, J.S., Peterson, D.L., Riley, K.L., Liu, Y.Q., Luce, C.H., 2016. A review of the relationships between drought and forest fire in the United States. Glob. Change Biol. 13275.

Liu, Y.Q., 2006. North Pacific warming and intense northwestern U.S. wildfires. Geophys. Res. Lett. 33, L21710.

Liu, Y.Q., Goodrick, S.L., Heilman, W., 2014. Wildland fire emissions, carbon, and climate: wildfire-climate interactions. For. Ecol. Manage. 317, 80–96.

Liu, Y.Q., Stanturf, J., Goodrick, S.L., 2010. Trends in global wildfire potential in a changing climate. For. Ecol. Manage. 259, 685–697.

Liu, Y.Q., Avissar, R., 1999. A study of persistence in the land-atmosphere system with a fourth-order analytical model. J. Clim. 12 (8), 2154–2168.

Liu, Z.H., Yang, J., Chang, Y., Weisberg, P.J., He, H.S., 2012. Spatial patterns and drivers of fire occurrence and its future trend under climate change in a boreal forest of Northeast China. Glob. Change Biol. 18, 2041–2056.

Lv, A.F., Tian, H.Q., Liu, M.L., Liu, J.Y., Melillo, J.M., 2006. Spatial and temporal patterns of carbon emissions from forest fires in China from 1950 to 2000. J. Geophys. Res. 111, D05313.

Marcos, R., Turco, M., Bedía, J., Llasat, M.C., Provenzale, A., 2015. Seasonal predictability of summer fires in a Mediterranean environment. Int. J. Wildland Fire 24, 1076-1084.

McArthur, A.G., 1967. Fire Behaviour in Eucalypt Forests. Department of National Development Forestry and Timber Bureau, Canberra, Leaflet, p. 107.

McKee, T.B., Doesken, N.J., Kleist, J., 1993. The relationship of drought frequency and duration of time scales. Eighth Conference on Applied Climatology, American Meteorological Society, Jan17-23, 1993, Anaheim CA, pp. 179-186.

Molina-Terrén, D.M., Xanthopoulos, G., Diakakis, M., Ribeiro, L., Caballero, D., Delogu, G.M., Viegas, D.X., Silva, C.A., Cardil, A., 2019. Analysis of forest fire fatalities in Southern Europe: Spain, Portugal, Greece and Sardinia (Italy). Int. J. Wildland Fire 28, 85–98.

Moritz, M.A., Batllori, E., Bradstock, R.A., Malcolm, G.A., Handmer, J., Hessburg, P.F., Leonard, J., McCaffrey, S., Odion, D.C., Schoennagel, T., Syphard, A.D., 2014. Learning to coexist with wildfire. Nature 515 (7525), 58–66.

Nagy, R.C., Fusco, E., Bradley, B., Abatzoglou, J.T., Balch, J., 2018. Human-related ignitions increase the number of large wildfires across U.S. ecoregions. Fire 1 (1), 4.

Osborn, T.J., Barichivich, J., Harris, I., Van der Schrier, G., Jones, P.D., 2017. Monitoring global drought using the self-calibrating Palmer Drought Severity Index [in "State of the Climate in 2016"]. Bull. Am. Meteorol. Soc. 98 (8), S32–S33.

Palmer, W.C., 1965. Meteorological drought. Weather Bureau Paper 45, US Dept. of Commerce, Washington D.C.

Potter, B.E., 2012. Atmospheric interactions with wildland fire behaviour-I. Basic surface interactions, vertical profiles and synoptic structures. Int. J. Wildland Fire 21 (7), 779–801.

Reddington, C.L., Morgan, W.T., Darbyshire, E., Brito, J., Coe, H., Artaxo, P., Scott, C.E., Marsham, J., Spracklen, D.V., 2019. Biomass burning aerosol over the Amazon: analysis of aircraft, surface and satellite observations using a global aerosol model. Atmos. Chem. Phys. https://doi.org/10.5194/acp-2018-849.

Schoennagel, T., Balch, J.K., Brenkert-Smith, H., Dennison, P.E., Harvey, B.J., Krawchuk, M.A., Mietkiewicz, N., Morgan, P., Moritz, M.A., Rasker, R., 2017. Adapt to more wildfire in western North American forests as climate changes. Proc. Natl. Acad. Sci. 114, 4582–4590.

Seager, R., Hooks, A., Williams, A.P., Cook, B., Nakamura, J., Henderson, N., 2015. Climatology, variability, and trends in the US vapor pressure deficit, an important fire-related meteorological quantity. J. Appl. Meteorol. Climatol. 54 (6), 1121–1141.

Sedano, F., Randerson, J.T., 2014. Multi-scale influence of vapor pressure deficit on fire ignition and spread in boreal forest ecosystems. Biogeosciences 11 (14), 3739–3755.

Shawki, D., Field, R.D., Tippett, M.K., Saharjo, B.H., Albar, I., Atmoko, D., Voulgarakis, A., 2017. Long-lead prediction of the 2015 fire and haze episode in Indonesia. Geophys. Res. Lett. 44, 1–10.

Spessa, A.C., Field, R.D., Pappenberger, F., Langner, A., Englhart, S., Weber, U., Stockdale, T., Siegert, F., Kaiser, J.W., Moore, J., 2015. Seasonal forecasting of fire over Kalimantan, Indonesia. Nat. Hazards Earth Syst. Sci. 15, 429–442.

Steelman, T., 2016. U. S. Wildfire governance as social-ecological problem. Ecol. Soc. 21 (4), 3.

Tian, X.R., Shu, L.F., Wang, M.Y., Zhao, F.J., 2017. The impact of climate change on fire risk in Daxing'anling, China. J. Forestry Res. 28 (5), 997–1006.

Tian, X.R., Shu, L.F., Zhao, F.J., Wang, M.Y., 2015. Dynamic Characteristics of Forest Fires in the Main Ecological Geographic Districts of China. Scientia Silvae Sinicae 51 (9), 71-77.

Tian, X.R., Zhao, F.J., Shu, L.F., Wang, M.Y., 2013. Distribution characteristics and the influence factors of forest fires in China. For. Ecol. Manage. 310, 460–467.

Tian, X.R., Zhao, F.J., Shu, L.F., Wang, M.Y., 2014. Changes in forest fire danger for south-western China in the 21st century. Int. J. Wildland Fire 23, 185–195.

Tian, X.R., Shu, L.F., Wang, M.Y., Jiao, M., 2003. Using Keetch-Byram Drought Index to forecast fire danger rating. Fire Safety Sci. 12 (3), 151–155.

Turco, M., Jerez, S., Doblas-Reyes, F.J., AghaKouchak, A., Liasat, M.C., Provenzale, A., 2018. Skilful forecasting of global fire activity using seasonal climate predictions. Nat. Commun. 9, 2718.

van der Schrier, G., Barichivich, J., Briffa, K.R., Jones, P.D., 2013. A scPDSI-based global data set of dry and wet spells for 1901–2009. J. Geophys. Res.: Atmos. 118, 4025–4048.

Van Wagner, C.E., 1987. Development and structure of the Canadian Forest Fire Weather Index System. Government of Canada, Canadian Forestry Service, Ottawa, Ontario Forestry Technical Report 35. 37 p.

Westerling, A.L., Gershunov, A., Brown, T.J., Cayan, D.R., Dettinger, M.D., 2003. Climate and wildfire in the western United states. Bull. Am. Meteorol. Soc. 595.

Westerling, A.L., Hidalgo, H.G., Cayan, R., Swetnam, T.W., 2006. Warming and earlier spring increase western U.S. forest wildfire activity. Science 313.

Yao, Q.C., Brown, P.M., Liu, S., Rocca, M.E., Trouet, V., Zheng, B., Chen, H., Li, Y., Liu, D., Wang, X., 2017. Pacific-Atlantic Ocean influence on wildfires in northeast China (1774 to 2010). Geophys. Res. Lett. 44 https://doi.org/10.1002/2016GL071821.

Ye, T., Wang, Y., Guo, Z., Li, Y., 2017. Factor contribution to fire occurrence, size, and burn probability in a subtropical coniferous forest in East China. PLoS ONE 12 (2), e0172110.

Yi, K.P., Bao, Y.L., Zhang, J.Q., 2017. Spatial distribution and temporal variability of open fire in China. Int. J. Wildland Fire 26, 122–135.

Zhang, Y.J., Qin, D.H., Yuan, W.P., Jia, B.R., 2016. Historical trends of forest fires and carbon emissions in China from 1988 to 2012. J. Geophys. Res. Biogeosci. 121, 2506–2517.

Zhao, F.J., Shu, L.F., Di, X.Y., Tian, X.R., Wang, M.Y., 2009. Changes in the occurring date of forest fires in the Inner Mongolia Daxing'anling forest region under global warming. Scientia Silvae Sinicae 45 (6), 166–172.

Zhao, F.J., Liu, Y.Q., Shu, L.F., 2020. Change in the fire season pattern from bimodal to unimodal under climate change: The case of Daxing'anling in Northeast China. Agric. For. Meteorol. 291, 108075.

Zhao, F.J., Liu, Y.Q., 2019. Atmospheric circulation patterns associated with wildfires in the monsoon regions of China. Geophys. Res. Lett. 46 (9), 4873–4882.

Zhou, L., Wu, J.J., Mo, X.Y., Zhou, H.K., Diao, C.Y., Wang, Q.F., Chen, Y.H., Zhang, F.Y., 2017. Quantitative and detailed spatiotemporal patterns of drought in China during 2001–2013. Sci. Total Environ. 589, 136–145.